AFRL-RX-WP-TR-2018-0080

EVALUATION OF A MELT INFILTRATED SIC/SIC CERAMIC MATRIX COMPOSITE

Larry P. Zawada
Universal Technology Corporation (UTC)

Jennifer L. Pierce
University of Dayton Research Institute (UDRI)

Craig P. Przybyla & Allan P. Katz
AFRL/RXCCP

20 DECEMBER 2017
Final Report

AIR FORCE RESEARCH LABORATORY
MATERIALS AND MANUFACTURING DIRECTORATE
WRIGHT-PATTERSON AIR FORCE BASE, OH 45433-7750
AIR FORCE MATERIEL COMMAND
UNITED STATES AIR FORCE

NOTICE AND SIGNATURE PAGE

Using Government drawings, specifications, or other data included in this document for any purpose other than Government procurement does not in any way obligate the U.S. Government. The fact that the Government formulated or supplied the drawings, specifications, or other data does not license the holder or any other person or corporation; or convey any rights or permission to manufacture, use, or sell any patented invention that may relate to them.

This report was cleared for public release by the USAF 88th Air Base Wing (88 ABW) Public Affairs Office (PAO) and is available to the general public, including foreign nationals.

Qualified requestors may obtain copies of this report from the Defense Technical Information Center (DTIC) (http://www.dtic.mil).

AFRL-RX-WP-TR-2018-0080 HAS BEEN REVIEWED AND IS APPROVED FOR PUBLICATION IN ACCORDANCE WITH ASSIGNED DISTRIBUTION STATEMENT.

//Signature//
CRAIG P. PRZYBYLA
Project Engineer
Composite Branch
Structural Materials Division
Materials and Manufacturing Directorate

//Signature//
TIMOTHY D. BREITZMAN
Branch Chief
Composite Branch
Structural Materials Division
Materials and Manufacturing Directorate

//Signature//
AMBER I. DAVIS
Deputy Division Chief
Structural Materials Division
Materials And Manufacturing Directorate

This report is published in the interest of scientific and technical information exchange, and its publication does not constitute the Government's approval or disapproval of its ideas or findings.

REPORT DOCUMENTATION PAGE

Form Approved
OMB No. 0704-0188

1. REPORT DATE *(DD-MM-YY)*	2. REPORT TYPE	3. DATES COVERED *(From - To)*
20 December 2017	Final	1 January 2009 – 20 November 2017

4. TITLE AND SUBTITLE
EVALUATION OF A MELT INFILTRATED SIC/SIC CERAMIC MATRIX COMPOSITE

5a. CONTRACT NUMBER
In-House

5b. GRANT NUMBER

5c. PROGRAM ELEMENT NUMBER
62102F

6. AUTHOR(S)
Larry P. Zawada –UTC
Jennifer Pierce – UDRI
Craig Przybyla and Allan Katz – AFRL/RXCC

5d. PROJECT NUMBER
4347

5e. TASK NUMBER

5f. WORK UNIT NUMBER
X0S7

7. PERFORMING ORGANIZATION NAME(S) AND ADDRESS(ES)
AFRL/RXCC
Materials and Manufacturing Directorate
2230 Tenth Street, Suite 1
Wright-Patterson AFB, OH 45433-7750

8. PERFORMING ORGANIZATION REPORT NUMBER
AFRL-RX-WP-TR-2018-0080

9. SPONSORING/MONITORING AGENCY NAME(S) AND ADDRESS(ES)
Air Force Research Laboratory
Materials and Manufacturing Directorate
Wright-Patterson Air Force Base, OH 45433-7750
Air Force Materiel Command
United States Air Force

10. SPONSORING/MONITORING AGENCY ACRONYM(S)
AFRL/RXCC

11. SPONSORING/MONITORING AGENCY REPORT NUMBER(S)
AFRL-RX-WP-TR-2018-0080

12. DISTRIBUTION/AVAILABILITY STATEMENT
Distribution Statement A. Approved for public release; distribution unlimited.

13. SUPPLEMENTARY NOTES:
PA Case Number: 88ABW-2017-5354; Clearance Date: 14 Nov 2017. This document contains color.

14. ABSTRACT (*Maximum 200 words*):
A dedicated experimental test program characterized the mechanical behavior of a melt infiltrated SiC/SiC ceramic matrix composite material at room and elevated temperature. This report describes tensile, creep, and fatigue testing procedures and presents the results.

15. SUBJECT TERMS
ceramic matrix composites, creep, dwell fatigue, fatigue, high temperature, melt infiltrated, SiC/SiC

16. SECURITY CLASSIFICATION OF:			17. LIMITATION OF ABSTRACT:	18. NUMBER OF PAGES	19a. NAME OF RESPONSIBLE PERSON (Monitor)
a. REPORT	b. ABSTRACT	c. THIS PAGE			Craig Przybyla
Unclassified	Unclassified	Unclassified	SAR	59	19b. TELEPHONE NUMBER *(Include Area Code)* (937) 255-9396

REPORT DOCUMENTATION PAGE Cont'd

6. AUTHOR(S)

Larry P. Zawada – UTC
Jennifer Pierce - UDRI
Craig Przybyla and Allan Katz – AFRL/RXCC

7. PERFORMING ORGANIZATION NAME(S) AND ADDRESS(ES)

Universal Technology Corporation
1270 North Fairfield Road
Dayton, Ohio 45432-2600

University of Dayton Research Institute
Structural Integrity Division
300 College Park
Dayton, OH 45469-0128

AFRL/RXCC
Composites Branch; Structural Materials Division
Materials and Manufacturing Directorate
2230 Tenth Street, Suite 1
Wright Patterson Air Force Base, OH 45433

TABLE OF CONTENTS

Section **Page**

LIST OF FIGURES

Figure **Page**

LIST OF TABLES

Table **Page**

1.0 SUMMARY

After two decades of research, ceramic matrix composites (CMCs) are finding their way into the hot sections of both military and civilian aerospace turbine engines. A detailed technical understanding of the high-temperature mechanical performance, as well as the identification of key damage mechanisms, is critical for a successful introduction of this new class of composite materials. Such information is vital for component design and for developing lifing methodologies such that component failures are avoided in service.

An experimental investigation into the high-temperature performance of a silicon carbide (SiC) fiber-reinforced silicon-carbide-matrix composite fabricated by General Electric (GE) Aviation was conducted. Test results and conclusions are presented.

2.0 INTRODUCTION

2.1 Background

Ceramic matrix composites are candidates for applications in future aerospace turbine engines, hypersonic platforms, and space access vehicles. Current engines have reached the upper limits of metallic hot section components. Therefore, CMCs are attractive replacements because of their high-temperature capability and density that is one-third that of nickel-based super-alloys. CMCs are relatively new, and little high-temperature performance data exists that was not generated by the CMC manufacturers. The ability to test and evaluate the high-temperature performance of a state-of-the-art CMC provides evidence that this new class of materials can, or perhaps cannot, meet the harsh thermomechanical service environment of an aerospace turbine engine. A technical understanding of the high-temperature performance of these new propulsion materials is required so that turbine engine designers can consider CMCs for turbine engines that power fighter aircraft, helicopters, and transports.

Applications include high-pressure turbine (HPT) shrouds for the next-generation T700 engine powering Apache, Seahawk, and Black Hawk helicopters. GE is also developing and using CMCs in commercial jet engines. With GE partner SAFRAN, CFM International's LEAP Engine (Leading Edge Aviation Propulsion) is the first commercial jet engine to use CMC shrouds in the HPT. This engine powers single aisle aircraft from Airbus, Boeing, and Comac. The GE9X engine that will power the next Boeing 777 expands CMC use to the inner and outer combustor liners, HPT Stage 1 and Stage 2 nozzles, and Stage 1 shrouds. GE is also testing CMCs in the GEnx demonstrator engine that will be run with CMC combustor liners, HPT Stage 1 shrouds, and HPT Stage 2 nozzles.

The CMC selected was developed and fabricated by GE Aviation and incorporates a SiC fiber reinforcing a SiC matrix (SiC/SiC) that utilizes the melt infiltration of silicon. Generating mechanical performance independent of the composite supplier allows for an impartial evaluation of a CMC that is nearing introduction in aerospace turbine engines. Data on this CMC had been generated under GE auspices alone, without third-party confirmation. First-hand knowledge of the CMC's high-temperature mechanical behavior was deemed essential for defense establishment personnel to understand CMC performance in service.

2.2 Program Objectives

The objective of this research was to determine the mechanical behavior of a state-of-the-art ceramic matrix composites that is a leading candidates for application in military and commercial turbine engine hot sections, and to do so independently of the materials supplier. CMCs for aerospace turbines are being actively pursued by the major turbine companies. But data is held tightly by these companies and their suppliers. Therefore independent confirmation is important and serves as a means for providing the CMC community performance test data outside the supply chain.

Testing of the GE SiC/SiC CMC was accomplished under conditions relevant to the aerospace turbine engine hot section. A unique set of high-temperature tensile and fatigue data is now

available. These test data provide an independent evaluation of the CMC material for comparison with the historical data sets for this CMC. Overall, the information presented in this report serves as an independent confirmation of the generally excellent high-temperature tensile and fatigue behavior offered by SiC/SiC CMCs.

3.0 PROCEDURES

3.1 Materials Description

An advanced CMC representative of those transitioning to military aerospace turbine engine components was identified by AFRL for study. It was an advanced state-of-the-art SiC/SiC CMC manufactured by GE Aviation.

AFRL purchased panels and pre-machined test specimens from GE. An agreement was reached between GE an AFRL that allowed for mechanical testing, non-destructive evaluation, and fracture surface analysis. The agreement required that no chemical composition analysis or detailed microstructural evaluation be conducted.

The SiC/SiC CMC purchased from GE for this study is designated Melt Infiltrated (MI) Gen 1.1 HiPerComp™ and utilizes an advanced silicon carbide fiber trade named Hi-Nicalon™. A schematic of the composite manufacturing process is shown in Figure 1. The composites were processed at GE Aviation's facility in Newark, Delaware, then named GE Ceramic Composite Products (GE-CCP).

The first composite fabrication step involves coating the fibers with a proprietary, boron nitride based coating. This coating is critical to achieving toughened composite mechanical behavior. The coated fibers are passed through a proprietary SiC-based slurry bath to infiltrate the fiber tow with the matrix precursor, and then wound on a mandrel to form a unidirectional tape. The tape is allowed to dry, removed from the drum, and cut to the desired sizes. Then the individual unidirectional tapes are stacked in the desired sequence and orientation to form a panel which is then debulked. The stacking sequence for this composite was 0-90-0-90-90-0-90-0, represented by (0/90)2s, meaning that the 0-90 is repeated twice and then the next four plies are symmetric to the first four plies (mirror image). After debulking, the assembly is fired at high temperature and then densified by infiltration with liquid silicon to produce the MI portion of the matrix. The silicon reacts with the matrix precursor to form SiC. The resulting composite matrix that surrounds the coated SiC fibers is mostly SiC, but with some remaining silicon metal.

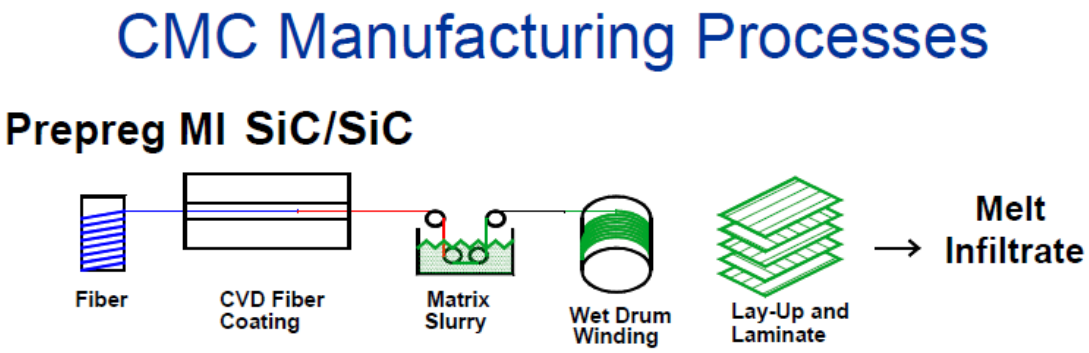

Figure 1. A simple schematic of the manufacturing process used to manufacture the CMC panel used in this study

The microstructure of the HiPerComp^{TM} Gen 1.1 Hi-Nicalon/SiC (0/90)2s was examined by preparing polished cross-sections of the CMC and viewing under an optical microscope. A specimen that had been tension-tested at room temperature was sectioned in the tab region. Cross-sections were prepared 90° to the length (axial direction) of the specimen and 45° to the length of the test specimen. The 0/90 orientation allowed for examining the microstructure and ply orientation and was important for studying in-plane matrix cracks. A challenge with 0/90 sections was that the fibers parallel to the cut-surface direction pulled out during polishing, precluding measurement of a true fiber volume fraction. But the cut and mounted specimens at the 45° orientation allowed for an accurate measure of fiber volume fraction.

An optical micrograph of the cross-section for the 0/90 orientation is shown in Figure 2 at a low magnification of 100×. The fibers appear circular for the 0° fiber plies and as cylinders for the 90° fibers. All eight plies can be easily identified in the image. Matrix-rich regions can be seen between all of the plies, and there are significant matrix-rich regions on both surfaces of the CMC. Figure 3 is an expanded view of Figure 2 and highlights the center section of the composite. From the image, the two 90° plies located at the center of the composite are clearly visible and the matrix region between the two center plies is very evident, even though these two plies are both 90°. Figure 4 is a 500× magnification image of the microstructure and focuses on one of the 0° plies, while Figure 5 is a much higher magnification (1000×) of a 0° tow. In Figure 5 one can see the fiber coating on the fibers, with the fibers near the outside of the tow having a thicker coating than those near the interior of the tow. The bright phase inside the fiber tows is residual silicon from the melt-infiltration process. The unreacted silicon fills up any voids or porosity. In this figure, one can also identify matrix cracks in the matrix-rich regions, which have also filled with silicon. It is the filling of pores and matrix cracks with silicon that results in a very dense matrix. Overall the composite microstructure is very uniform, and there is a complete lack of any observable porosity.

Figure 2. Optical micrograph of HiPerComp™ Gen 1.1 Hi-Nicalon/SiC (0/90)2s showing a 0/90 cross-section at 100×

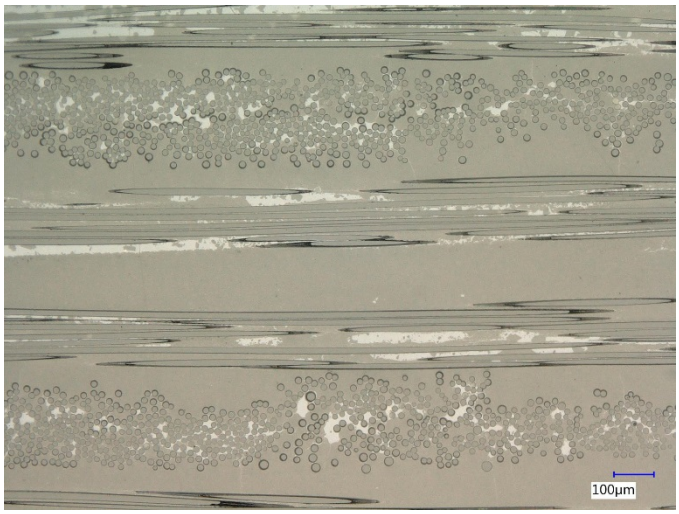

Figure 3. Optical micrograph of HiPerComp™ Gen 1.1 Hi-Nicalon/SiC (0/90)2s showing a 0/90 cross-section at 200×

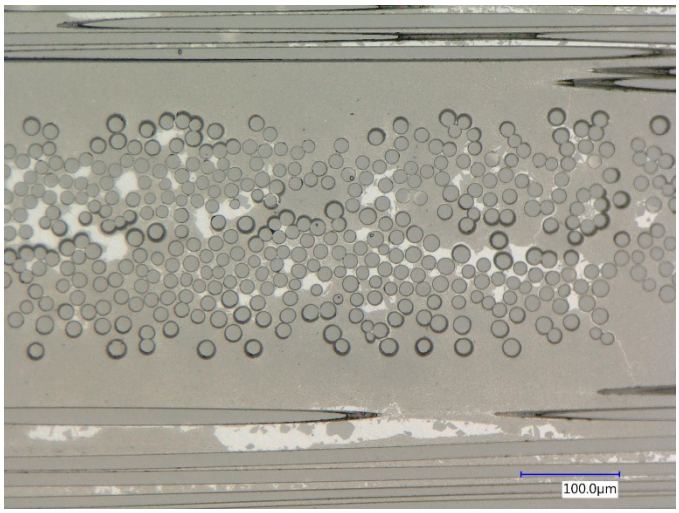

Figure 4. Optical micrograph of HiPerComp™ Gen 1.1 Hi-Nicalon/SiC (0/90)2s showing a 0/90 cross-section at 500×

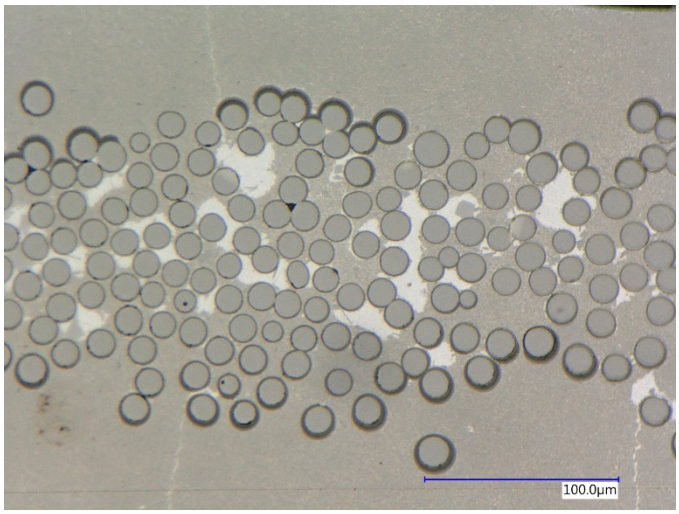

Figure 5. Optical micrograph of HiPerComp™ Gen 1.1 Hi-Nicalon/SiC (0/90)2s showing a 0/90 cross -section at 1000×

A micrograph of the cross-section taken of the ±45 orientation is shown in Figure 6 at a low magnification of 100×. Since all fibers are oriented 45° to the polished surface, there is no fiber pull-out. The micrograph gives a true representation of the fiber distribution within the composite. Figure 7 is a 200× image of the 45° microstructure, and one can observe that the fiber volume fraction in each ply varies significantly along the width. Figure 8 is a 500× micrograph, and Figure 9 is a 1000× micrograph of the 45° microstructure. It is apparent that some fibers have a much thicker fiber coating than others, and that there are a significant number of silicon-rich areas that are 1 to 5 fiber diameters in size. In Figure 9, one can clearly see that there was a processing crack that ran horizontally through this fiber bundle and that it has completely filled with silicon. Even at this extremely high magnification, there is no sign of any

residual porosity or open-matrix cracks. It is this very dense matrix that gives this CMC very good high-temperature performance.

Figure 6. Optical micrograph of HiPerComp™ Gen 1.1 Hi-Nicalon/SiC (0/90)2s showing a ±45 cross-section at 100×

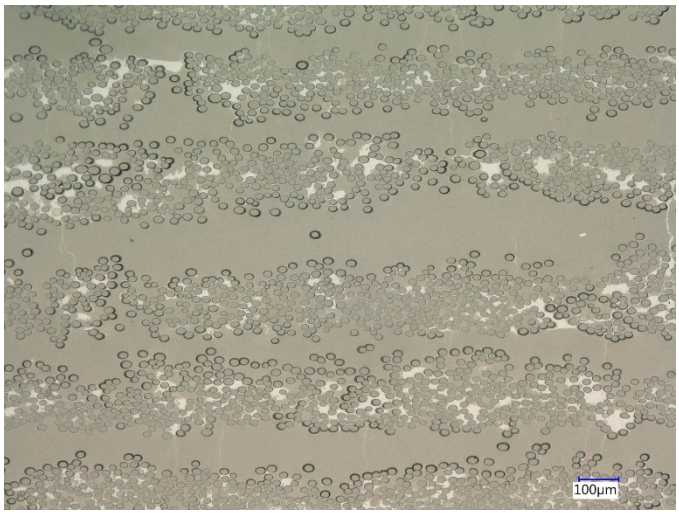

Figure 7. Optical micrograph of HiPerComp™ Gen 1.1 Hi-Nicalon/SiC (0/90)2s showing a ±45 cross-section at 200×

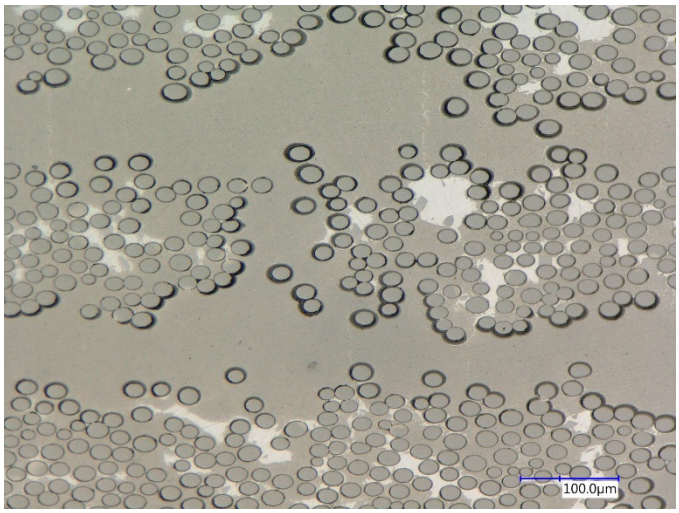

Figure 8. Optical micrograph of HiPerComp™ Gen 1.1 Hi-Nicalon/SiC (0/90)2s showing a ±45 cross-section at 500×

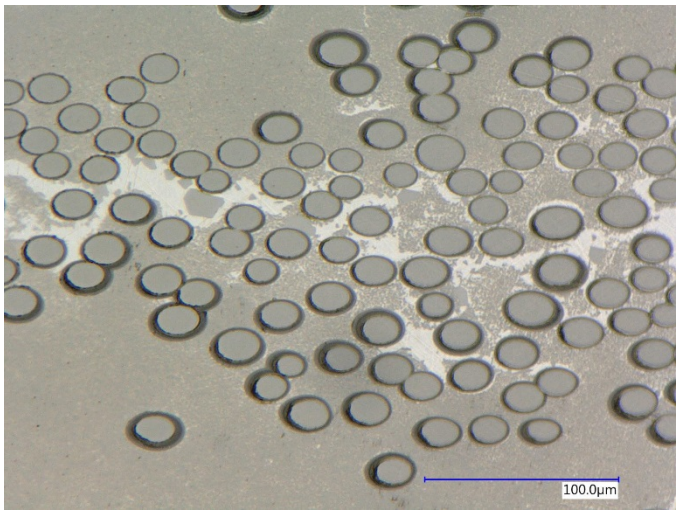

Figure 9. Optical micrograph of HiPerComp™ Gen 1.1 Hi-Nicalon/SiC (0/90)2s showing a ±45 cross-section at 1000×

A photograph of an as-manufactured panel is shown in Figure 10. The top corners of each panel were notched as seen in the photograph to identify the direction of the fibers on the surface. This was important, because the test specimens were oriented such that the fibers in the surface ply were parallel with the loading axis of the specimen. With both notches at the top, the orientation of the fibers was parallel with the loading axis of the specimen, vertically from top to bottom.

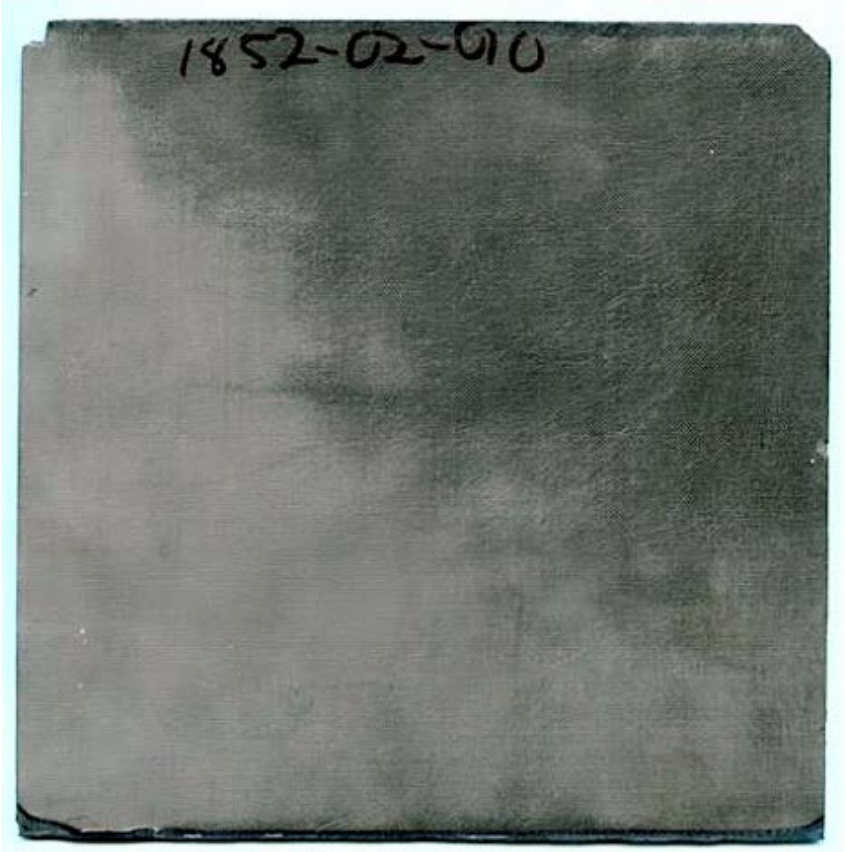

Figure 10. Optical photograph of an as-produced panel. The upper corners were notched to indicate the direction of the surface fibers. In this image, the surface ply fibers run from the top to the bottom of the panel.

3.2 Purchase and Machining of CMC Panels

A total of 20 panels of dimensions 158.8 mm × 158.8 mm × eight plies thickness were manufactured in two lots of 10 panels each. Unidirectional plies were laid up $(0/90)_{2s}$ to form the eight-ply composite panels. A small witness panel was made with each lot, such that room-temperature tensile tests could be performed. These witness tests were necessary, as the purchase order specified that the CMC panels meet minimum physical properties and a required panel flatness. These minimums were an ultimate tensile strength (UTS) of 38 ksi (262 MPa), a proportional limit (PL) of 18 ksi (124 MPa), a modulus of 38 ksi (262 GPa), and a panel flatness of 0.010″ (0.25 mm) over 4 inches. Non-destructive evaluations using infrared (IR) thermography were performed on all of the panels. In addition to the room temperature tension tests, General Electric also conducted a few tension tests at 1204°C and 1316°C and supplied that data along with the room temperature test data.

A total of 10 panels were initially machined by GE into the appropriate dogbone test specimen geometry. Great care was taken to mark each panel to identify where each test specimen was situated on the panel. A photo of a panel marked for machining is shown in Figure 11 while Figure 12 shows a drawing of the dogbone test specimen. Ten dogbone test specimens were machined from each panel as shown in Figure 13. The remaining 10 panels were held in reserve. Once additional planning was done, seven of the remaining panels were sent out to be machined into dogbone test specimens.

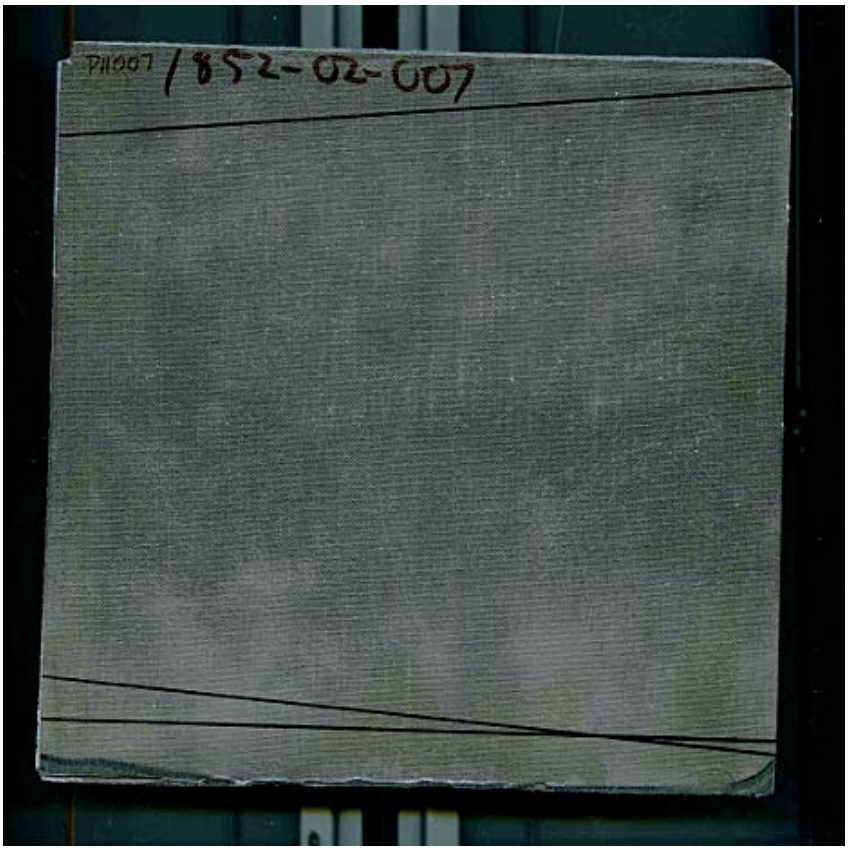

Figure 11. Optical photograph of a CMC panel shown with identification markings in preparation for machining into dogbone test specimens

3.3 Specimen Geometry

A dogbone specimen geometry was selected for all tensile and durability testing and is shown in Figure 12. Overall specimen length of 150 mm (6″) was selected, as it allowed for different furnace configurations to fit between the cooled test system grips. A 28 mm (1.1″) straight section was selected to accommodate high-temperature extensometers with ceramic extension rods that typically have either a 12.5 mm (0.5″) or 25 mm (1″) gage length. The radius of curvature used for the transition region between the gage section and the specimen tab was 305 mm (1.97″). A finite-element stress analysis of the test specimen geometry documented that this radius creates a stress concentration that is only approximately 1% higher than in the straight section. This large radius greatly reduces the stress concentration, but greatly increases the

length of the radius section. Increasing the length of the radius allows the section along the taper to be outside the hot zone of the furnace and exposed to intermediate temperatures. This in turn can lead to intermediate temperature embrittlement (ITE), which can be caused by oxidation mechanisms around 900°C. The radius geometry was justified by prior experience with this CMC, which has shown that ITE does not occur. The absence of ITE is attributed to a high-quality fiber coating and very dense matrix.

As stated above, General Electric machined ten panels for a total of 100 dogbone test specimens and AFRL sent out 7 of the remaining panels to an alternate vendor to be machined into dogbone test specimens. Specimens from the first two panels received were found to have gage lengths shorter than specified. The shop was so informed, and the remaining five panels were machined correctly while specimens from the first two panels were sent back to the machine shop and machined to the correct gage length. A total of 17 panels were machined into dogbone specimens and produced 170 dogbone test specimens.

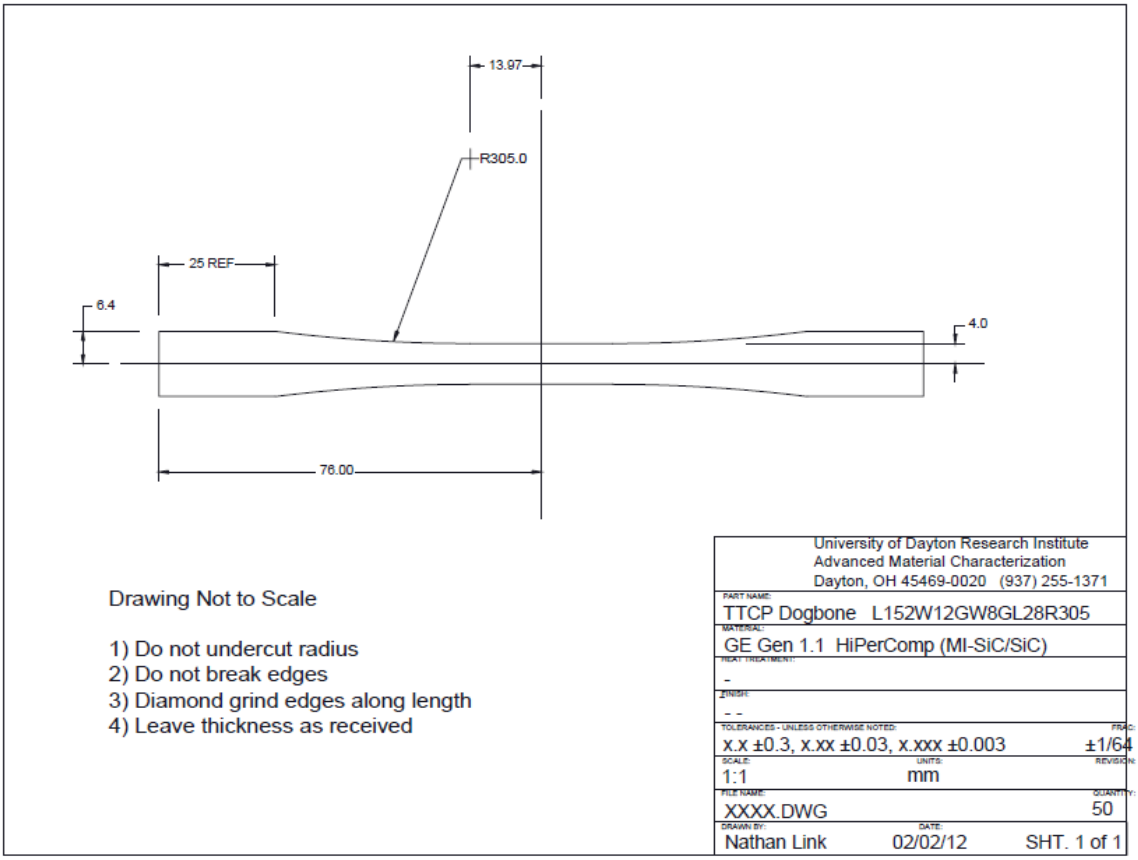

Figure 12. Drawing of the dogbone test specimen used for all tension, fatigue, and creep rupture tests

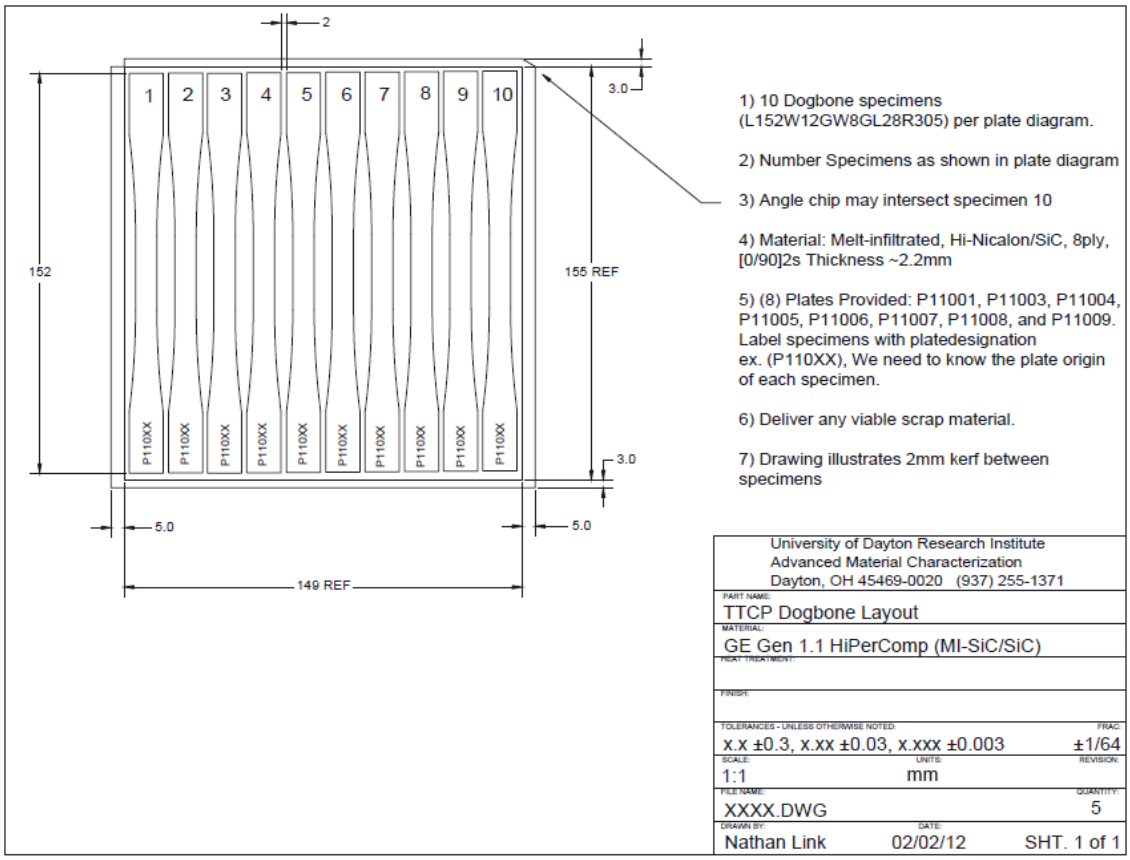

Figure 13. Machining drawing for a panel showing the layout of the dogbone test specimens on the panel

3.4 Acceptance Criteria: NDE

As part of the purchasing acceptance criteria, all 20 panels were scanned using an infrared (IR) technique that provides both through-thickness in-plane IR images and transmission IR thermal diffusivity. All 20 easily passed this IR evaluation. In fact, these IR scans highlighted that the 20 panels were of exceptional quality, with no indications of porosity or delaminations. A typical IR scan is shown in Figure14 as reflection IR depth images for both faces of the panels and in Figure 15 as a transmission IR thermal diffusivity image. In viewing the reflection IR images, one can see the panel is very uniform.

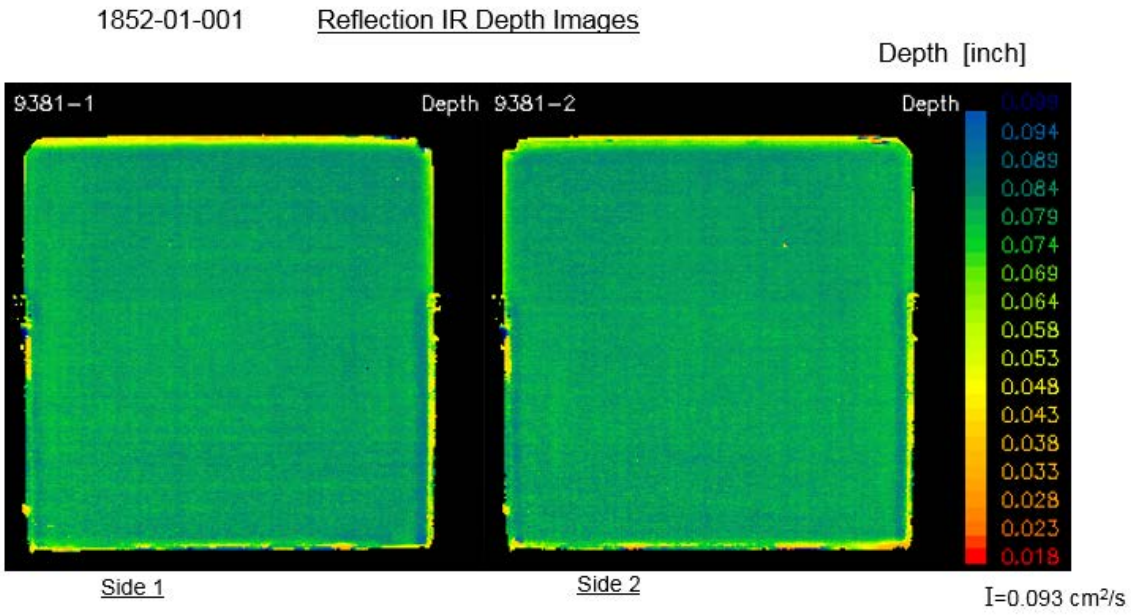

Figure 14. Reflection infrared depth images taken from each side of one of the panels. Panel scans were exceptionally uniform.

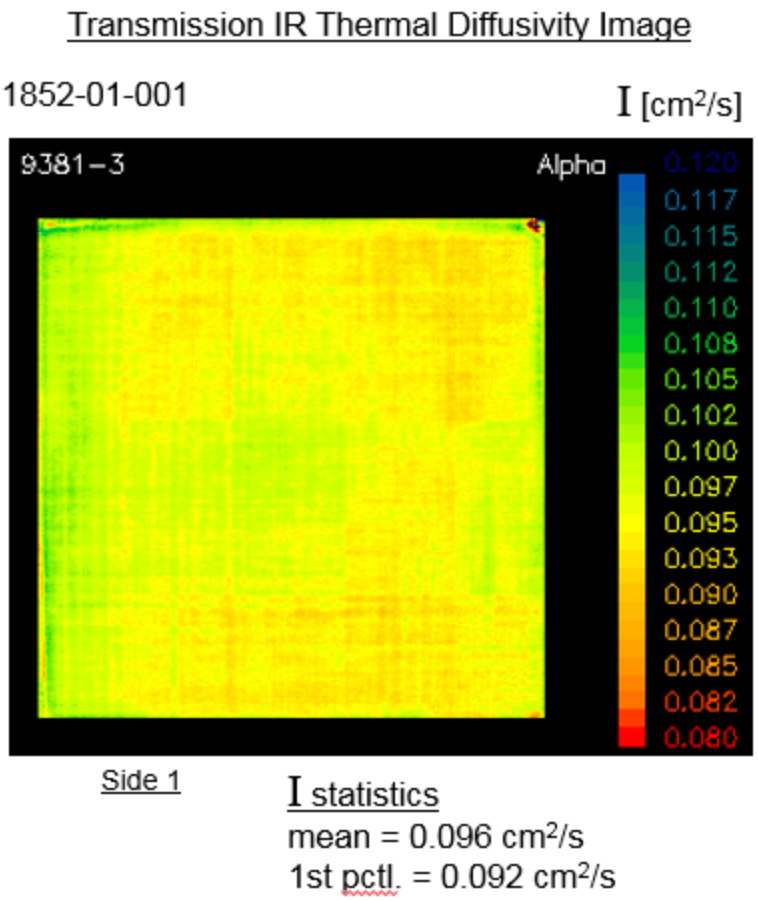

Figure 15. Transmission infrared thermal diffusivity image of one panel. Note the exceptional uniformity of the scan.

3.5 Acceptance Criteria: Panel Flatness

In addition to NDE, the purchase request required the panels to pass a flatness test. This was made a criterion since it is known that the liquid silicon infiltration process can lead to significant residual stresses. In the past these stresses have resulted in the warping of thin panels such as those employed in this study. The requirement was that the specimens could bow no more than 0.25 mm (0.010″) over 100 mm length (4”). All of the panels met this flatness specification.

3.6 Acceptance Criteria: Room-Temperature Tensile Properties

As stated earlier in section 3.2, GE was required to conduct verification testing prior to delivery of the test specimens. Minimum room-temperature tensile properties were specified in the purchase order. In addition to performing room-temperature tension tests, GE also conducted elevated-temperature tension tests. Table 1 shows reference data published by GE citing typical properties that could be expected for the GE SiC/SiC using the Hi-Nicalon fibers. The nomenclature PP-HN (the CMC for this study) indicates prepregged Hi-Nicalon and the SC-HN indicates slurry-cast Hi-Nicalon. Significant gains have been made in manufacturing these

silicon melt-infiltrated SiC/SiC CMCs. In the table, the expected ultimate tensile strength (UTS) was shown to be 48 ksi (331 MPa), the proportional limit (PL) was 26 ksi (179 MPa), and the modulus was 41 ksi (283 MPa).

With this information, and in discussions with GE, the purchase order required the witness coupons to demonstrate a minimum UTS of 38 ksi (262 MPa), a PL of 18 ksi (124 MPa), and a modulus of 38 ksi (262 GPa). A technical decision was made to exclude a minimum specification on strain to failure, since its value can vary significantly depending on the location of the extensometer with respect to the failure location during the test. Current component designs for CMC limit the operating stress to below the PL to avoid any matrix cracking. Therefore, the primary concern was stiffness and PL.

Table 1.Typical Properties for GE Melt-Infiltrated CMC Materials from Product Brochure #GEA-13712 (1/04)

CMC Material Properties - MI Products

Property	Unit	Melt Infiltration (HIPerComp TM)					
		PP-HN		SC-HN		SC-Sylramic	
		73°F	2200°F	73°F	2200°F	73°F	2200°F
In-plane Ultimate Tensile Strength (UTS)	ksi	48	33	52	39		45
Strain at Failure	%	0.9	0.3	0.7	0.5		0.5
In-plane Proportional Limit Strength	ksi	26	24	17	19		24
In-plane Tensile Modulus	Msi	41	35	28	21		26
Interlaminar Tensile Strength	ksi	6					
Interlaminar Shear Strength	ksi	20	18				7 (1500°F)
In-plane Thermal Conductivity	BTU/h-ft-°F	18	8	17	(6)		
Through-thickness Thermal Conductivity	BTU/h-ft-°F	13	7	10	(5)		
In-plane Thermal Expansion Coefficient	10^{-6}/°F	2.3	2.3	2.1	2.9		
Through-thickness Thermal Expansion Coefficient	10^{-6}/°F	2.3	2.3	1.7	1.5		
Density	g/cm^3	2.8		2.7		2.8	

The CMC material properties expressed herein are preliminary estimates based on technical data considered reliable by GE Energy. Such material property information is intended for persons having technical skill in CMC or related technologies and is provided without charge or obligation. Any use of the information is at the user's own risk and discretion. GE Energy makes no warranties, either express or implied, and assumes no liabilities in connection with any use of this information or with the long-term availability of the specific CMC materials described herein. Nothing herein shall be taken as an offer to license or a recommendation to infringe the intellectual property rights of others.

The room-temperature tensile stress-strain behavior for the witness panel coupons are shown in Figure 16, while the 1204°C (2200°F) data are shown in Figure 17, and the 1316°C (2400°F) data are shown in Figure 18. A plot combining all of the tensile tests is shown in Figure 19. The same data in Figure 19 is once again presented in Figure 20, but with the room-temperature traces in black, the 1204°C traces in blue, and the 1316°C traces are in red to make it easier to compare the data. All of the tensile test properties are listed in Table 2.

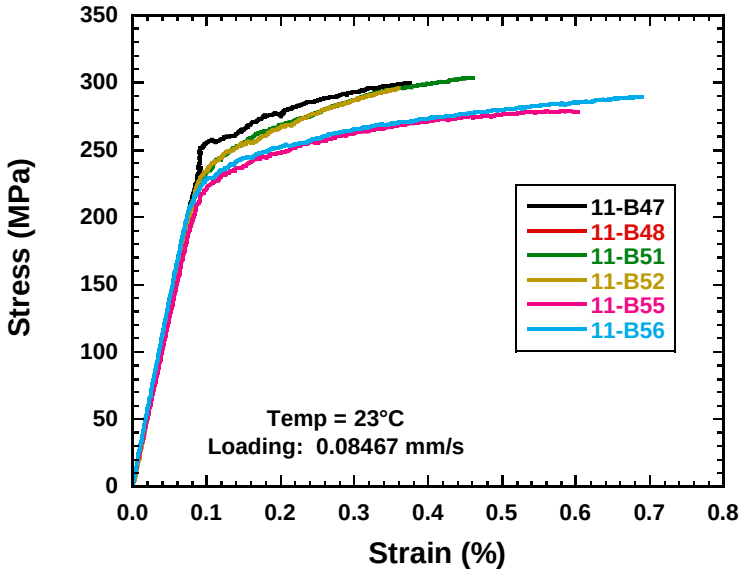

Figure 16. Tensile stress-versus-strain traces for GE-CCP Melt-Infiltrated Gen 1.1 HiPerComp™ Hi-Nicalon/SiC (0/90)2s CMC witness panels tested at room temperature

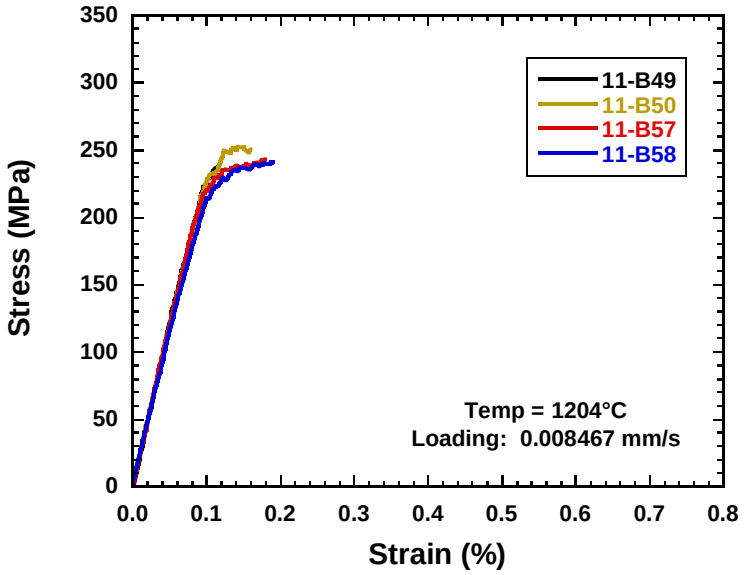

Figure 17. Tensile stress-versus-strain traces for GE-CCP Melt-Infiltrated Gen 1.1 HiPerComp™ Hi-Nicalon/SiC (0/90)2s CMC witness panels tested at 1204°C

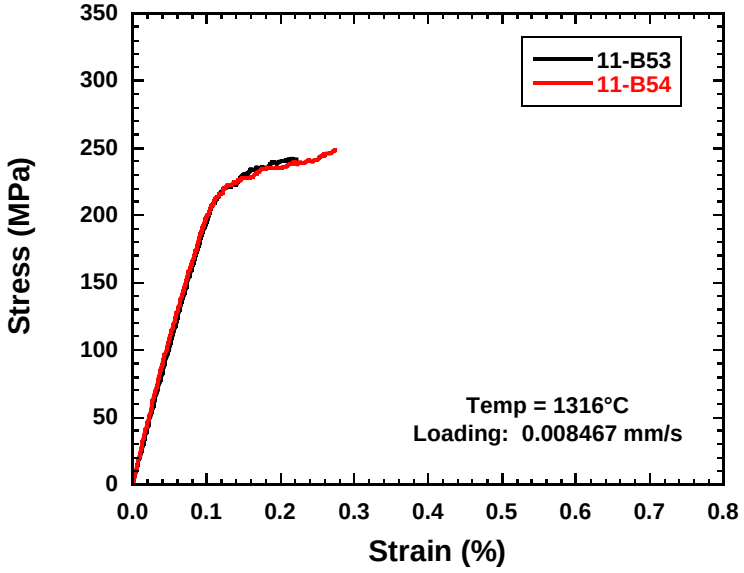

Figure 18. Tensile stress-versus-strain traces for GE-CCP Melt-Infiltrated Gen 1.1 HiPerComp™ Hi-Nicalon/SiC (0/90)2s CMC witness panels tested at 1316°C

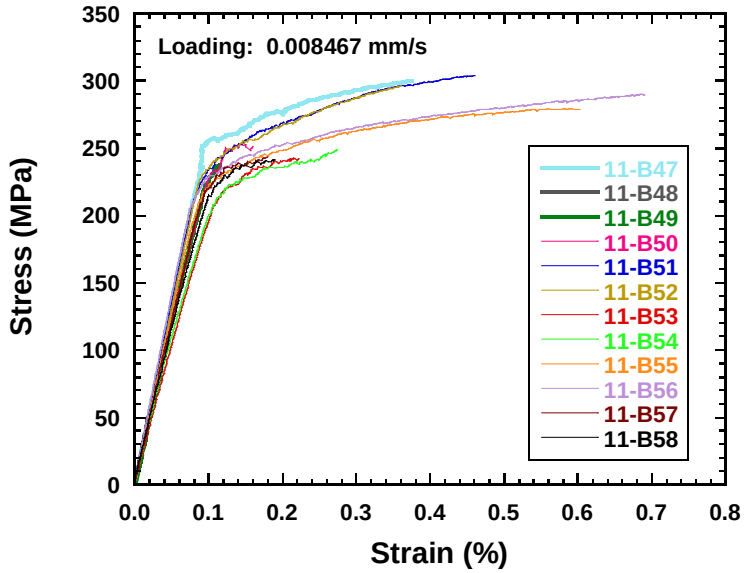

Figure 19. Combo tensile stress-versus-strain traces for GE-CCP Melt-Infiltrated Gen 1.1 HiPerComp™ Hi-Nicalon/SiC (0/90)2s CMC witness panels tested at 23°C, 1204°C, and 1316°C

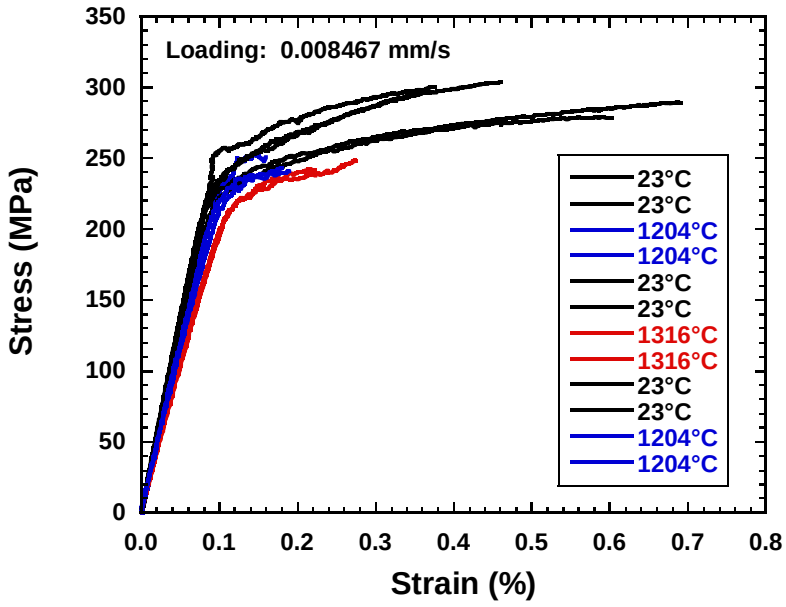

Figure 20. Witness tensile stress-versus-strain traces for GE-CCP Melt-Infiltrated Gen 1.1 HiPerComp™ Hi-Nicalon/SiC (0/90)2s CMC witness panels tested at 23°C (black) 1204°C (blue traces), and 1316°C (red traces)

Table 2. Tabulated Tensile Data for the Witness Coupon Tests Conducted by General Electric

GE-CCP Specimen Number	Test Temperature (C)	Air Force Specimen Number	UTS (MPa)	Modulus (5-25 MPa) (GPa)	PL (10% offset) (MPa)	Strain to Failure (%)	Failure Type
1852-01-010-02-L1	23	11-B47	300.1	269.7	257.1	0.38	RA-T
1852-01-010-02-L2	23	11-B48	305.7	272.7	228.7	0.48	RA-T
1852-02-010-02-L1	23	11-B51	303.6	270.3	226.7	0.46	GAGE
1852-02-010-02-L2	23	11-B52	296.0	268.6	233.7	0.36	RA-T
1852-01-0012-02-L1	23	11-B55	279.0	247.1	220.1	0.60	GAGE
1852-01-0012-02-L2	23	11-B56	289.5	284.8	210.6	0.69	RA-B
		Average	295.6	268.9	229.5	0.5	
		Stdev	10.01	12.22	15.71	0.13	
1852-01-010-02-L3	1204	11-B49	237.5	257.8	223.1	0.12	RA-B
1852-01-010-02-L4	1204	11-B50	252.7	239.0	232.0	0.16	RA-T
1852-01-0012-02-L3	1204	11-B57	243.2	230.6	224.8	0.18	GAGE
1852-01-0012-02-L4	1204	11-B58	241.2	229.2	214.1	0.19	RA-B
		Average	243.6	239.1	223.5	0.2	
		Stdev	6.49	13.16	7.37	0.03	
1852-02-010-02-L3	1316	11-B53	242.3	210.9	207.4	0.22	GAGE
1852-02-010-02-L4	1316	11-B54	248.5	224.5	166.9	0.27	RA-T
		Average	237.2	221.1	195.1	0.31	

RA-T: Failure Near Radius At Top
RA-B: Failure Near Radus At Bottom

The room-temperature tension stress-versus-strain traces shown in Figure 16 overlap up to a stress of approximately 210 MPa. Tabulated results in Table 2 show that the room-temperature modulus ranged from a low of 247 GPa to a high of 284 GPa. One coupon exhibited a modulus below the required stiffness of 262 GPa, but the remaining five coupons were above the threshold and it was decided that this was acceptable. Modulus can be dependent on the range over which it is calculated and, for this investigation, that was between 5 MPa and 25 MPa. Such a small range of stress and strain does introduce some scatter, as this is at the very low end of most extensometers used to measure strain. In addition, the value was within 10% of the average modulus measured for each specimen, and this is an accuracy check used by AFRL when measuring modulus. Above 210 MPa there appeared to be scatter in the stress at which the stress-strain trace deviated from linearity. This deviation is where the PL is identified. Looking at the results shown in Table 2, the room-temperature PL varied from a low of 210 MPa to a high of 257 MPa. These values easily exceeded the specified PL of 124 MPa. It was very important that the panels met this criterion, as the PL is the stress at which significant matrix cracking begins to occur. After the PL was reached, there was extensive non-linear stress-strain response, and the curves no longer overlap but rather exhibit varying amounts of strain to failure. But the lowest strength recorded was 279 MPa, and this exceeded the 262 MPa specification. Therefore, with the exception of the one modulus value, all witness panel test data met or exceeded the specified room-temperature properties.

From the data at 1204°C shown in Figure 17, it is clear that the specimen traces overlap to the PL, with very little additional strain after the PL was reached. The data presented in Table 2

clearly show that the modulus, PL, and UTS all decreased at 1204°C versus room temperature. Such results suggest that, even for these fast-fracture tests, the stress-strain response exhibits temperature effects.

The results of the two tests at 1316°C are presented in Figure 18. The two traces were almost identical, and strain to failure increased versus at 1204°C. However, the modulus decreased significantly, along with the PL (see Table 2).

All of the test data are plotted in Figure 19 and in Figure 20 as color-coded stress-strain traces to make it easier to observe subtle differences in the stress-strain behavior. In viewing the figures it is clear that at temperatures of 1204°C and higher, there is a pronounced temperature effect. Therefore the test data clearly demonstrate that for this CMC with a Hi-Nicalon fiber, the upper temperature limit even in fast fracture is below 1204°C. Therefore, most of the testing in this investigation was carried out at 1093°C (2000°F).

3.7 Test Plan

During the planning stage for this project, GE was consulted on test data and test temperatures that would be most relevant and important for this CMC. With due consideration creep rupture, fatigue, and dwell fatigue testing were selected to address time-dependent and cyclic-dependent behavior.

3.7.1 Test Matrix

Table 3 describes the initial test matrix that was planned. During the course of testing some adjustments were made to the plan to maximize benefit of data to be taken after analysis of the initial test results.

Table 3. AFRL Test Matrix

AFRL Test Matrix										
Test Type	Specimen Geometry	Stress Parameter	Temperature				SUB TOTAL	Spares	TOTAL	Objectives
			RT	982°C	1093°C	1204°C				
Temperature Mapping	DB L152W12GW8GL18R267	None		Y	Y	Y	1	0	1	Determine settings for furnace controllers and temperature distribution across materials
Tensile	DB L152W12GW8GL18R267	Failure	1	1	1	1	4	4	8	1) Determine baseline properties (RT) for material pedigree / lot 2) Determine tensile properties at Ts
Fatigue	DB L152W12GW8GL18R267	S1 = 210 MPa			1		1	2	3	Determine Cyclic Behavior
		S2 = 220 MPa			1		1	2	3	
		S3 = 230 MPa			1		1	2	3	
Creep Rupture	DB L152W12GW8GL18R267	S1 = 210 MPa			1		1	2	3	Determine Time Dependent Behavior
		S2 = 220 MPa			1		1	2	3	
		S3 = 230 MPa			1		1	2	3	
Dwell Fatigue Dwell Times: 10, 100, 1000 sec	DB L152W12GW8GL18R267	S1 = 210 MPa			1		1	2	3	Determine Dwell Hold Time Effect
		S2 = 220 MPa			1		1	2	3	
		S3 = 230 MPa			1		1	2	3	
						Specimen Totals	14	22	36	

AFRL Test Parameters
1) Material = GE-CCP Prepreg MI Hi-Nicalon/SiC
2) All materials [0/90]s layup, 8 plys, composite thickness ~ 0.08"
2) Specimen Geometry: DB L152W12GW8GL18R267 - The specimens to be tested by AFRL are not the standard, these were not machined to requeste
3) Tensile Test Rate: Load control, 10 MPa/s
4) Fatigue Parameters: Load controal, R=0.1, freq = 1 Hz, Run out = 27.7 hrs (N=100,000)
5) Dwell Fatigue Parameters: hold time at max stress is variable, 1 Hz unload-load, R=0.1, Run out = 27.7 hrs (N=variable)
6) MTS High Temperature Extensometer 0.5" GL (5% range - expected strain is up to 0.5%)

3.7.2 Baseline Tensile Properties

The intent of this study was to document the high-temperature performance of a new generation of CMC. In-plane tension tests were selected to determine the baseline properties of this new CMC. In-plane tensile tests on cross-ply (0/90) materials generate the basic design properties such as modulus (E), ultimate tensile strength (UTS), proportional limit (PL), and strain at failure (ε_f), as well as stress-strain behavior. Tensile tests provide information on both the linear-elastic behavior, as well as the non-linear damage-induced behavior. Beyond the elastic behavior, it is important to document the initial onset and subsequent non-linear stress-versus-strain response. This non-linear behavior develops as a result of a cumulative damage process that involves multiple concurrent damage mechanisms. These damage mechanisms can include matrix cracking, fiber-matrix debonding, oxidation of constituents in the CMC, crack growth, viscoelastic deformation, delamination, etc. In-plane tension tests were performed at both room (23°C) and elevated temperatures of 982°C (1800°F), 1093°C (2000°F), and 1204°C (2200°F). These tests were conducted according to the methods outlined in American Society for Testing and Materials (ASTM) Standards C1275 and C1359, for room and elevated temperature respectively. The tension tests were critical for determining the appropriate maximum temperature that would be used for all of the durability tests.

3.7.3 Durability Behavior

Tests under the "Durability Behavior" portion of the test matrix were selected to evaluate this CMC's ability to endure conditions of relevant temperature, environment, stress, and time. Testing regimes included fatigue, creep rupture, and dwell fatigue.

3.7.3.1 Fatigue Testing

Data from the tension tests was used to guide the selection of an appropriate initial stress level for conducting the fatigue tests. The objective of the fatigue testing was to determine the highest stress that could reach run-out. The initial starting stress level was selected to be approximately 10% below the PL stress. If the first specimen failed, the stress would be dropped 10 MPa. If rather the specimen ran out, the next test would be conducted at a stress level 10 MPa higher. The fatigue testing was used to determine if this CMC experiences cyclic damage and fatigue crack growth. Tests were conducted at a load ratio of 0.01 (min load/max load) and a frequency of 1 Hz. Run-out was determined to be 100,000 cycles (100,000 seconds) and equates to the projected maximum time at maximum temperature for modern military aerospace turbine engines. All specimens that ran out were cooled to room temperature and tension tested to determine the retained strength. Any changes in the tensile stress-strain response would indicate that damage had been introduced into the test specimen. Testing was conducted in accordance to ASTM Standard C1360 for fatigue testing of CMCs.

3.7.3.2 Creep Rupture Testing

Creep rupture testing followed the fatigue testing. The initial starting stress levels were based on the highest stress level to reach run-out during fatigue testing. Creep rupture testing is important, as it is used to identify time-dependent behavior. Test time to reach a run-out condition was selected to be the same length of time as the fatigue run-out condition (100,000 seconds). Any

specimens that ran out were cooled to room temperature and tension tested to determine the retained strength.

3.7.3.3 Dwell Fatigue Testing

The third set of tests involved dwell fatigue testing with the dwell applied at the maximum load of the fatigue cycle. Adding hold times at maximum load allowed for identifying interactions between time-dependent behavior and cyclic behavior. The goal was to determine if there was any evidence of a coupling effect between the two types of behavior. Hold times of 10 seconds, 100 seconds, and 1000 seconds were selected. Each hold time test had a different limit for the number of cycles to reach run-out, such that the total test time was to be 100,000 seconds.

The test matrix was presented in Table 3 and describes the initial types of tests and number of test specimens. Very few replicates were planned due to the high cost of the test specimens. The goal was not to generate a database, but to determine the active damage mechanisms.

3.7.4 Test Equipment Description

3.7.4.1 Test System: SH#12

Room- and elevated-temperature tests were performed using a horizontal Materials Test Systems (MTS) servo-hydraulic test machine (SH#12). A photograph of the test stand is shown in Figure 21. This test frame is uniquely orientated in the horizontal configuration and is equipped with custom-designed, water-cooled, friction-clamping grips; a MTS 609 alignment device; a 5.5-kip (25kN) MTS load cell; a MTS 458 analog Micro-Console signal controller; and UDRI-developed MATE (material analysis and testing) test control and data acquisition software. This test frame was designed and built in the horizontal configuration specifically for characterization of the high-temperature mechanical properties of CMCs, which demonstrate less than 1% strain to failure. Furnaces that operate in the vertical position experience “chimney” effects where the hot air rises and cooler air is drawn in from the bottom of the furnace. This can make it difficult to maintain a uniform temperature profile along the gage section of the test specimen. In a vertical arrangement, the lower end of the gage section is always cooler than the top end. Multiple heating zones and strategic placement of insulation can mitigate some of this effect. In contrast, furnaces operated with specimens in the horizontal orientation produce a very symmetric and uniform temperature profile across the gage section of the specimen. The horizontal configuration is also conducive to high-temperature strain measurement. The high-temperature extensometer mounting design requires substantially less spring force to keep the extensometer in contact with the test specimen, compared to when it is mounted in the vertical configuration.

Other features to note on this test frame are the unique gripping system and the custom control and data-acquisition software. The grips were designed in-house at AFRL to achieve a high degree of alignment while providing a fixed clamping condition at both ends of the specimen, ideal for strain-limited materials. These unique grips use a clamping action, driven by a pneumatic-to-hydraulic ram inside a yoke that goes around the grips, and applies the pressure normal to the grips. The grips require appropriately sized and prepared metal inserts to closely match the thickness of the test specimen such that the grips flex less than a few thousandths of an inch. Once aligned the system maintains alignment, and subsequent alignment checks are

extremely repeatable. The inserts are either sandblasted or coated with a rough coating to maximize the coefficient of friction between the test specimen and the grip inserts. The grip bodies are cooled while the metal inserts in contact with the specimen are not directly cooled. An MTS Model 609 device is used to align these grips by removing concentricity and angularity.

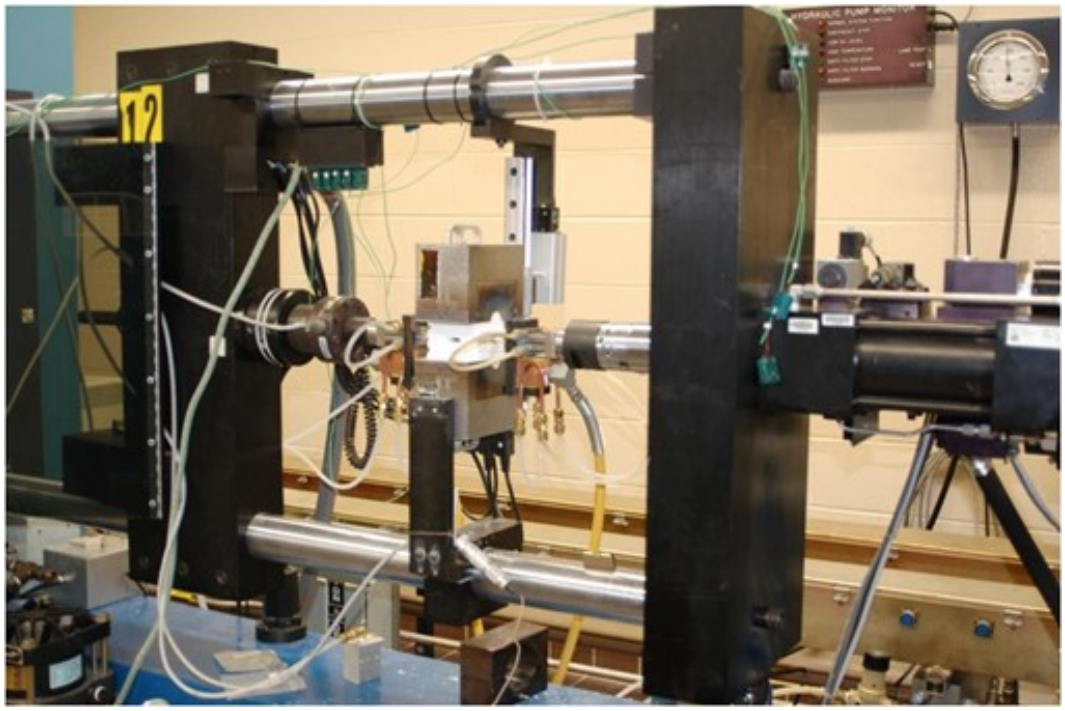

Figure 21. Photograph of the horizontal servo-hydraulic test system (SH#12) used for room- and elevated-temperature testing

3.7.4.2 Verification of Alignment

The grip/load train alignment was verified using a highly ground, hard steel, straight-sided specimen instrumented with eight strain gages, as shown in Figure 22. The goal for alignment was to be within ASTM specifications of less than 5% bending at 500 με displacement in all four specimen orientations. A plot of percent bending versus axial load is shown in Figure 23. Often, the percent bending at the aforementioned ASTM specification was about only 2%.

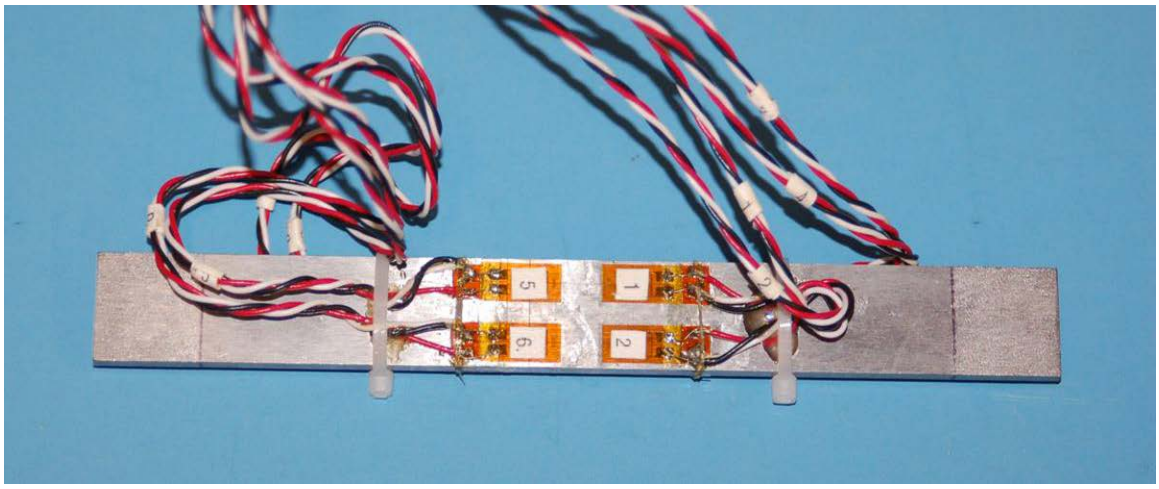

Figure 22. Strain gaged steel alignment specimen used to verify alignment of SH#12

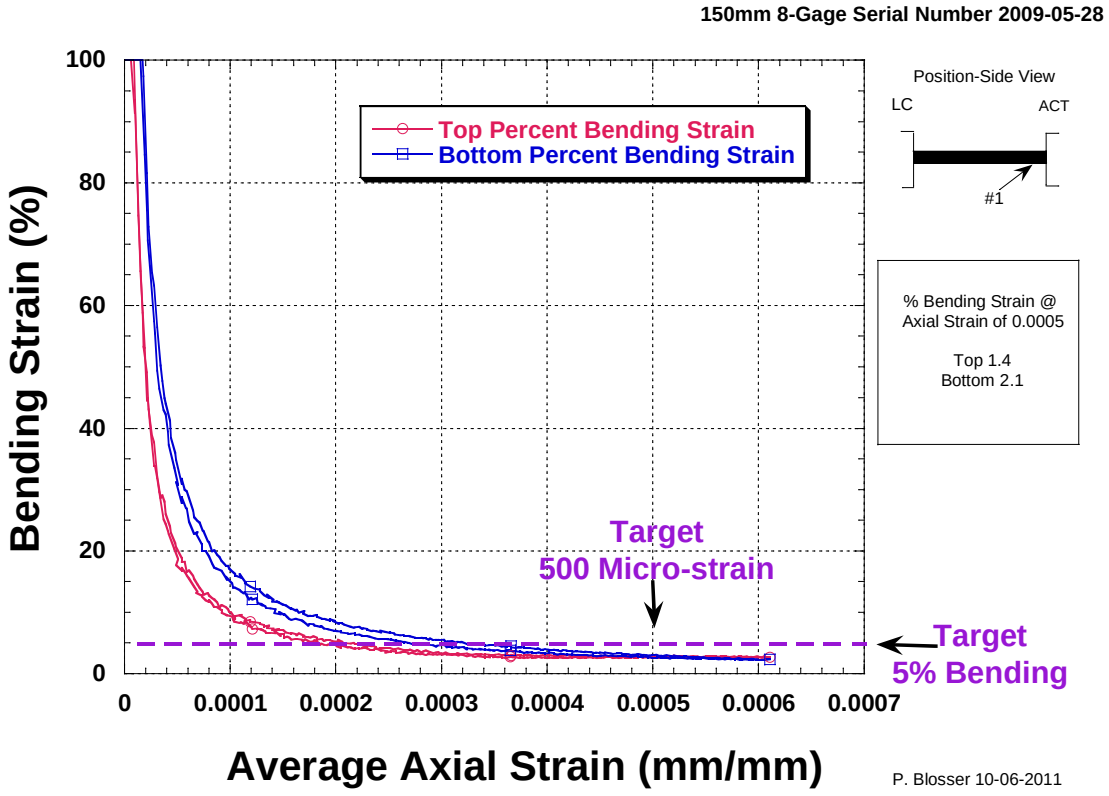

Figure 23. Plot of bending strain versus average axial strain for alignment check of SH#12

Testing was conducted using custom software developed by UDRI. The software program is called MATE and uses operator input along with the dynamic feedback from the load cell and extensometer to control the test and acquire test data including load, extensometer displacement, actuator stroke, time, and temperature. Calculations, such as engineering stress and strain, are reported automatically in the output file with all the measured inputs for load, displacement, time, and actuator positon.

3.7.4.3 Verification of Furnace Thermal Profile

Elevated-temperature testing was conducted using a commercially available 3-zone furnace made by Amteco, Incorporated. This split-design furnace uses three silicon-carbide heating elements in each furnace half. The heating elements are similar to the ignitor elements used in house furnaces. There are three S-type control thermocouples within the furnace cavity allowing for three zones of temperature control. Insulation with specimen and instrumentation cut-outs were placed between the two furnace halves to help preserve the integrity of the furnace cavities and help keep the furnace well-sealed. Having the furnace in a horizontal position allowed for the use of these easily replaced insulation cutouts.

Prior to starting this testing program, the furnace temperature set points were determined for the desired specimen temperatures. For all high-temperature testing, it is very important to calibrate the furnace using an actual test specimen and not just a thermocouple probe. Therefore, one SiC/SiC test specimen was dedicated to mapping the temperature profile across the gage length and determine the corresponding furnace set-point temperatures required to operate the furnace in an automated control mode. The test specimen was instrumented with thermocouples across the extensometer gage length, as well as outside the specimen gage length, as depicted schematically in Figure 24. The exact location of the thermocouples relative to the center of the specimen were 0 mm, -7 mm, +7 mm, -14 mm, and +22 mm. Great care was taken to locate the thermocouples on the temperature calibration specimen such that there was no twist to the thermocouple wires. They were attached to the calibration specimen with “B”-type wire ties, and then cemented in place with a ceramic adhesive. This technique has been documented to provide a more accurate temperature reading than just using a temperature probe in the furnace. Photographs of a specimen set for temperature profile measurement are shown in Figure 25 and Figure 26. The furnace set points were adjusted to achieve temperatures across the extensometer gage length that were within 1% of the target temperature. Figure 27 shows a plot of temperature versus location along an actual test specimen. Plotted in the figure are actual temperature of the test specimen and the temperature of each of the three zones in the furnace. The data shows that one cannot simply use the thermocouples located inside this type of furnace to accurately measure temperature on the specimen. Documentation of the furnace set points allowed for automatic control of the furnace temperature using the furnace thermocouples without having to mount thermocouples to the CMC test specimen. This eliminated any chance of having an adverse reaction between the thermocouple or bonding material and the CMC test specimen.

Strain was measured using either a 12.7 mm gage length MTS high-resolution model 632.26B-40 clip-on extensometer calibrated at 0.089 mm per 10 volts for room-temperature testing or a 15 mm gage length MTS 632.50B-04 high-temperature alumina rod extensometer calibrated at 0.1278 mm per 10 volts. Strategically placed insulation around the furnace and extensometer rods was required

to minimize effects of the thermal radiation that cause distortion in the rods and produces noise in the strain signal. A low-pressure air stream was passed through a diffuser and pointed at the body of the extensometer during high-temperature measurements to create a constant environment around the extensometer body.

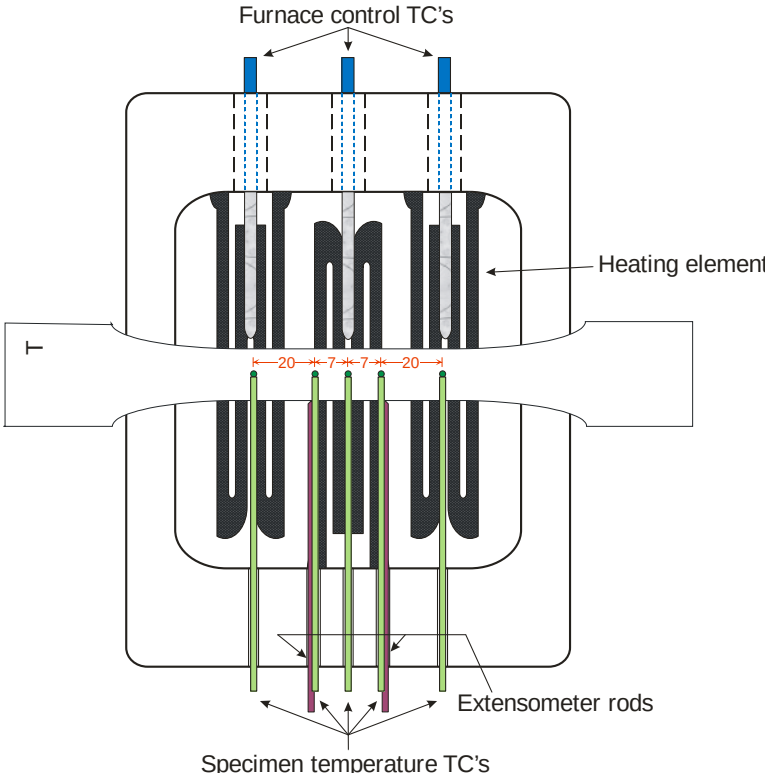

Figure 24. Schematic drawing showing the placement of the thermocouples for furnace temperature mapping

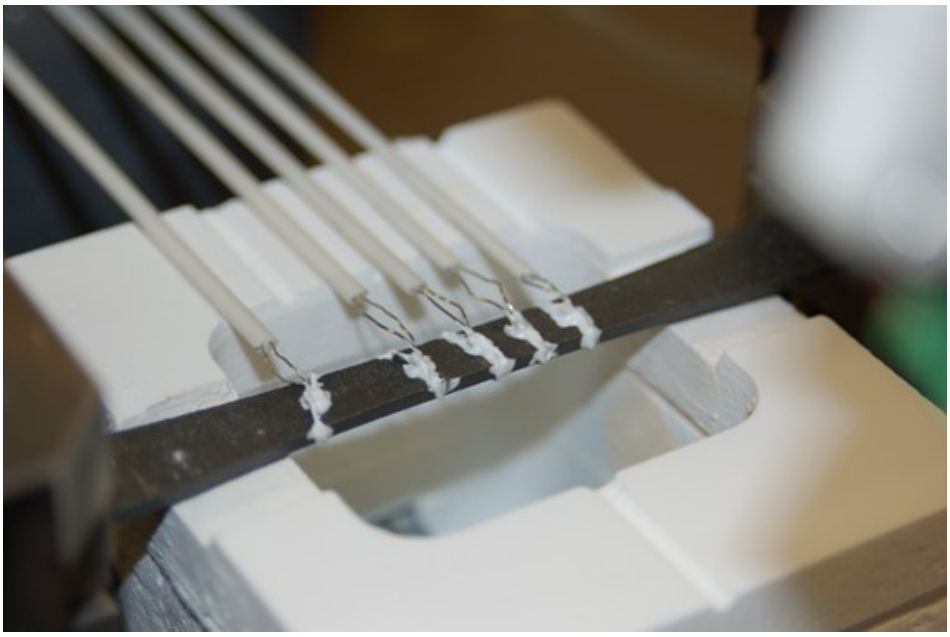

Figure 25. Photo of a CMC test specimen instrumented with thermocouples for furnace temperature mapping

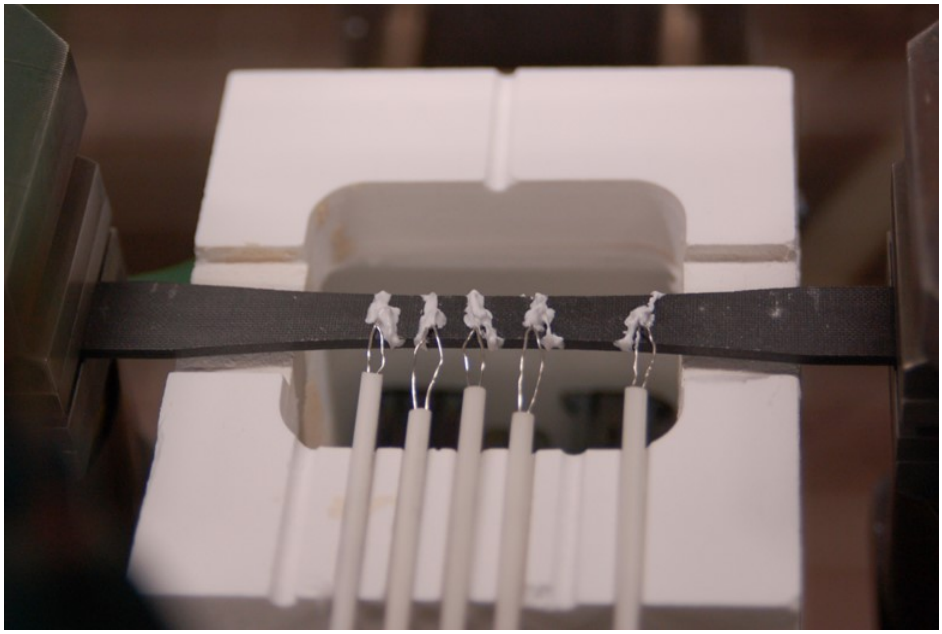

Figure 26. Photo of a CMC test specimen instrumented with thermocouples for furnace temperature mapping

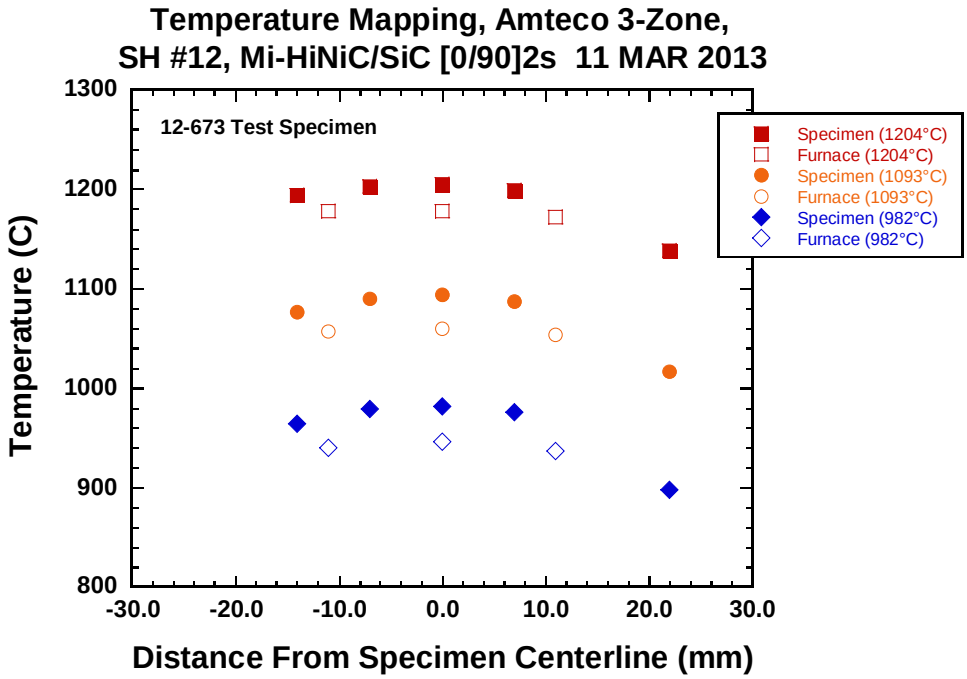

Figure 27. Temperature profile conducted on a GE Gen 1.1 Mi-HiNiC/SiC test specimen

4.0 RESULTS

4.1 Tensile Results

The first series of tests were conducted in tension at room and elevated temperatures of 982°C, 1093°C, and 1204°C. Only one specimen was tested at each temperature. The purpose of these tests was to identify the temperature at which the CMC stress-versus-strain trace starts to exhibit noticeable changes versus room temperature response. A plot of the tensile stress-versus-strain behavior for the four test temperatures is shown in Figure 28. Data from those four tension tests are presented in Table 7. As shown in the stress-versus-strain behavior in Figure 28, the response is very linear up to approximately 200-210 MPa. All four traces are almost identical, although the 1204°C trace appears to be slightly more compliant. The data in Table 7 reveal that the modulus decreased 10% at 1093°C and 14% at 1204°C. The PL stress remained constant up to 1204°C. However, the test at 1204°C exhibited very little strain after reaching the PL with a total strain to failure of only 0.12%. This is the key piece of information needed for the durability experiments. The primary objective was to push this CMC to as high a test temperature as possible while still exhibiting some strain after reaching the PL. Results from the test at 1093°C showed that, at this temperature, the CMC exhibited good strain to failure of approximately 0.321%. However, the CMC tested at 1204°C exhibited a significant decrease in strain to failure with very little strain after reaching the PL, then dropping to only 0.119% at failure. Therefore, a temperature of 1093°C was selected for all durability tests.

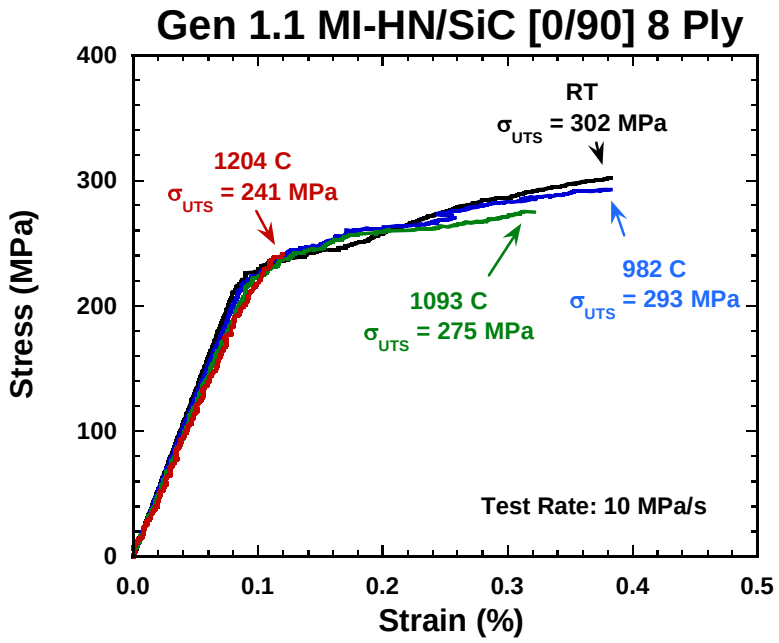

Figure 28. Tensile behavior for HiPerComp™ Gen 1.1 Hi-Nicalon/SiC (0/90)2s material tested at various temperatures

Table 4. Tensile Results for HiPerComp™ Gen 1.1 Hi-Nicalon/SiC (0/90)2s Material

TTCP Gen1.1 MI-Hi-Nicalon/SiC						
Specimen ID	**Temp. (C)**	**σ_{UTS} (MPa)**	**E (GPa)**	**σ_{PL} (MPa)**	**ε_f (%)**	**Failure Site* (mm)**
12-672	**23**	**302**	**267**	**227**	**0.382**	**18**
12-676	**982**	**293**	**254**	**224**	**0.383**	**13**
12-677	**1093**	**275**	**238**	**225**	**0.321**	**12**
12-682	**1204**	**241**	**230**	**220**	**0.119**	**5**

*Note: Failure Location from centerline of specimen. Right or left of centerline not recorded.

4.2 Durability Results

Durability tests performed included creep rupture, fatigue, and dwell fatigue. For the dwell fatigue testing, the dwell was applied at maximum load. The initial test stress of 210 MPa was chosen based on results from GE witness coupon test data and the aforementioned tension tests. (As previously noted, GE processed a panel additional to those purchased by AFRL, and they reported data against AFRL specifications for tensile behavior and flatness.) The objective was to select a stress level approximately 10 MPa below the PL which, from the tension test at 1093°C, was determined to be 225 MPa.

4.2.1 Fatigue Results

A total of three fatigue tests were conducted, all at 1093°C and the results are shown in Figure 29. The first two samples tested at 210 MPa failed in approximately 3000 seconds (~1 hour). Therefore, the stress level was decreased to 200 MPa and the specimen ran out. These test results established the fatigue limit, so no further tests were conducted.

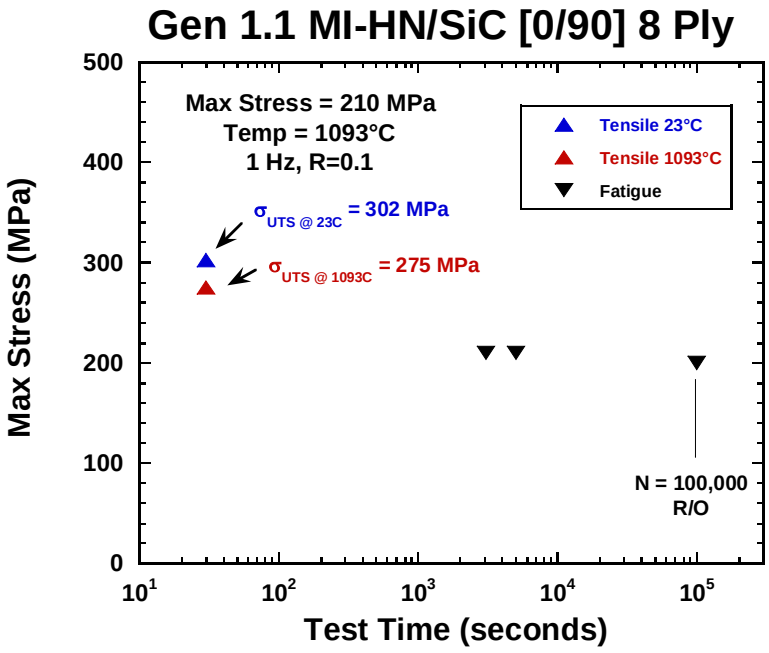

Figure 29 Maximum fatigue stress plotted against log time to failure in seconds for HiPerCompTM Gen 1.1 Hi-Nicalon/SiC (0/90)2s

4.2.2 Creep Rupture Results

Results from the fatigue tests guided the stress levels selected for creep rupture testing at 1093°C. It was decided that, since the fatigue test at 200 MPa ran out, the creep rupture tests would start at a 210 MPa. The reason for this is SiC/SiC CMCs often exhibit shorter lives in fatigue than during static loading. All four tests were conducted at a stress of 210 MPa and the results are shown in Figure 30. Three specimens reached run-out and one failed at approximately two hours. This behavior mimicked the fatigue behavior. The test specimens ran out or failed in a relatively short period of time. So, as with the fatigue testing, the creep rupture diagram is very flat with a creep rupture limit of approximately 2.5 MPa.

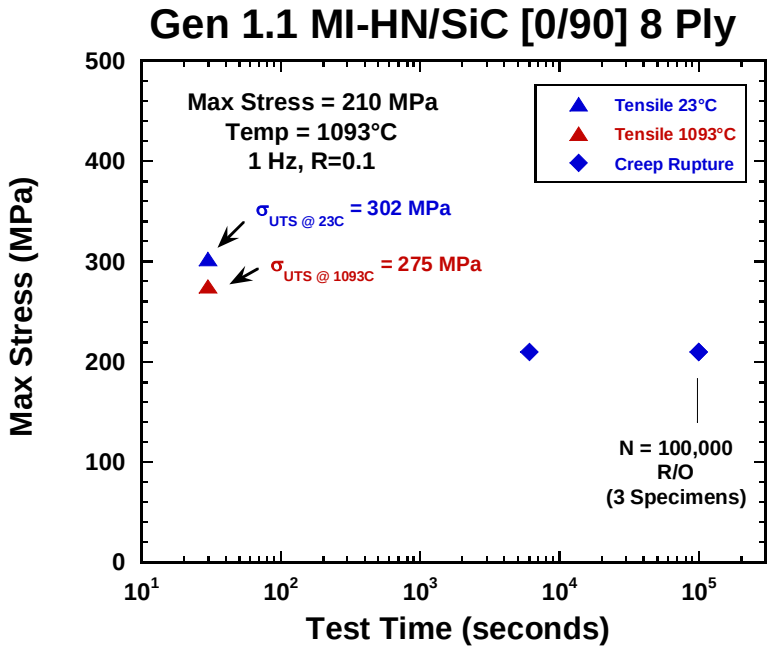

Figure 30. Creep stress plotted against log time to failure in seconds for HiPerComp™ Gen 1.1 Hi-Nicalon/SiC (0/90)2s

4.2.3 Dwell Fatigue Results

After reviewing the fatigue and creep results, it was decided that the dwell fatigue tests at 1093°C would be conducted only at a stress of 210 MPa. Two tests were performed with a hold time of 10 seconds, two with a hold time of 100 seconds, and four specimens were tested with a hold time of 1000 seconds. The results are shown in Figure 31. These test data showed no trends with respect to the hold times. All but one of the specimens failed in under five hours, with several failing in under one hour. One 10-second hold test and one 1000-second hold test ran out. This, again, highlights that the specimens either failed early or ran out, making for a very flat dwell fatigue-versus-time diagram. From these limited data, there appears to be no interaction between creep and fatigue for this CMC. In addition, the duration of the hold time does not appear to alter durability behavior. As with the fatigue and creep testing, the durability limit for the dwell fatigue tests was identified to be 205 MPa.

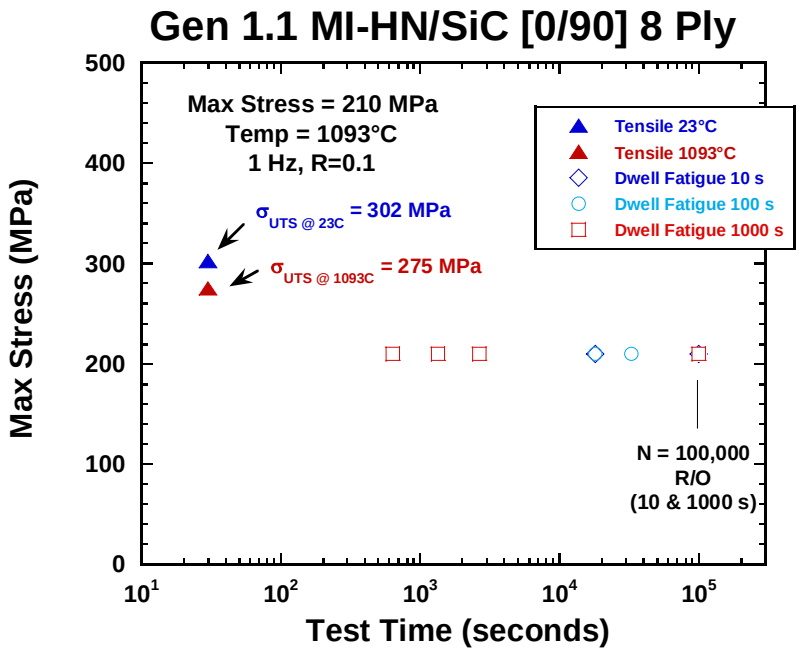

Figure 31. Maximum Dwell Fatigue stress plotted against log time to failure in seconds for HiPerComp™ Gen 1.1 Hi-Nicalon/SiC (0/90)2s

5.0 DISCUSSION OF TEST RESULTS

5.1 Tensile Behavior

The stress-versus-strain response is very similar to the witness test data supplied by GE. The room-temperature test results were nearly identical to the GE results with UTS, PL, and modulus all within 2%. The results at 1204°C also agreed well. GE measured a UTS of 241 MPa, a PL of 223 MPa, and a strain to failure of 0.2%. The test results reported here match well in regards to UTS, PL, and strain to failure, but a slightly lower modulus (by 4%) was measured. However, this is within the normal scatter for modulus in CMCs. The results for GE at 1204°C for strain to failure were 0.2%; whereas 0.1% was measured in this study. Both of these data sets identify a debt in strain to failure when tension tested at 1204°C. Therefore, a temperature of 1093°C was selected for all of the creep, fatigue, and dwell fatigue testing.

5.2 Creep Rupture Strain Behavior

For the creep rupture tests, both time to failure and strain as a function of time were recorded. Creep strain versus time is presented for the three run-out specimens in Figure 32, Figure 33, and Figure 34. For all four creep rupture tests the maximum creep strain measured was only 0.02%. There was 0.01% initial strain for the primary creep region, and then the strain remained relatively constant. Data for one run-out specimen, shown in Figure 32, exhibited approximately 0.01% strain increase, while the other two run-out specimens exhibited a slight decrease in creep strain. This decrease was an artifact of the strain-gage-based extensometer used for this study. The environment around the extensometer was not controlled. When test specimens do not experience any creep, the extensometer has been documented to drift slightly depending on the room environment. Therefore, the specimen did not shrink and the results are purely an artifact of the displacement measuring device. The measured strains are below the stability threshold of the extensometer.

The creep strain for the failed specimen is shown in Figure 35. The strain behavior of this specimen was not significantly different than the three specimens that failed. However, Figure 36 plots total strain versus time for the specimen that failed. From this plot, we can observe that the test specimen experienced strain that is very close to the strain limit associated with the PL. The data in Figure 36 is expanded in Figure 37. In this plot, one can clearly see that, near the maximum load, there is a small but noticeable sharper increase in strain. This can also be observed in Figure 38 as a plot of stress versus strain. This suggests that the PL has been exceeded and likely explains why this specimen failed while the other three reached run-out.

The creep strain data suggests that the failure did not result from significant strain deformation. The specimen that failed exceeded the PL and experienced nonlinear strain near maximum load. The main finding from studying the creep strain is that this CMC experienced very little creep strain during the 100,000-second tests at 1093°C.

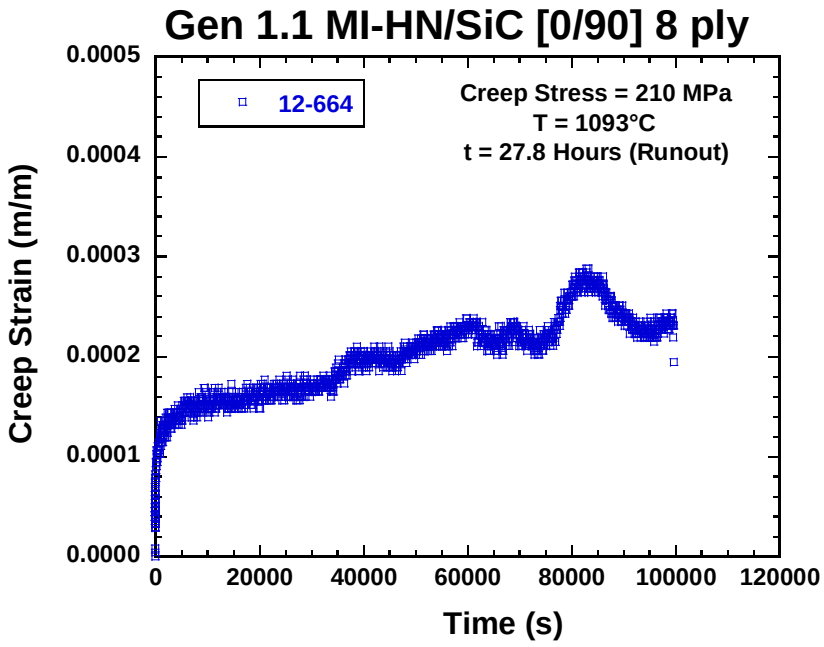

Figure 32. Creep strain versus time at 1093°C for a HiPerComp™ Gen 1.1 Hi-Nicalon/SiC (0/90)2s creep rupture run-out specimen

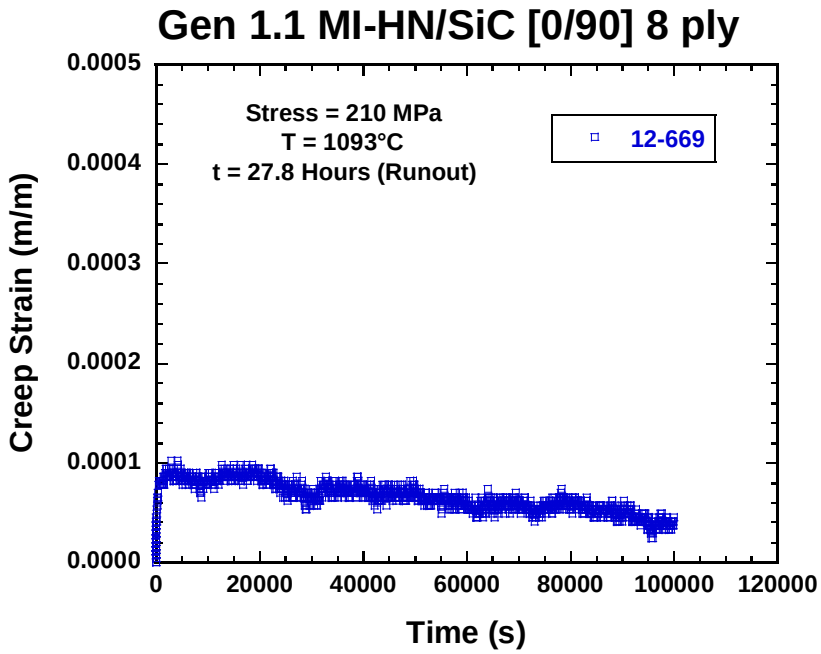

Figure 33. Creep strain versus time at 1093°C for a HiPerComp™ Gen 1.1 Hi-Nicalon/SiC (0/90)2s creep rupture run-out specimen

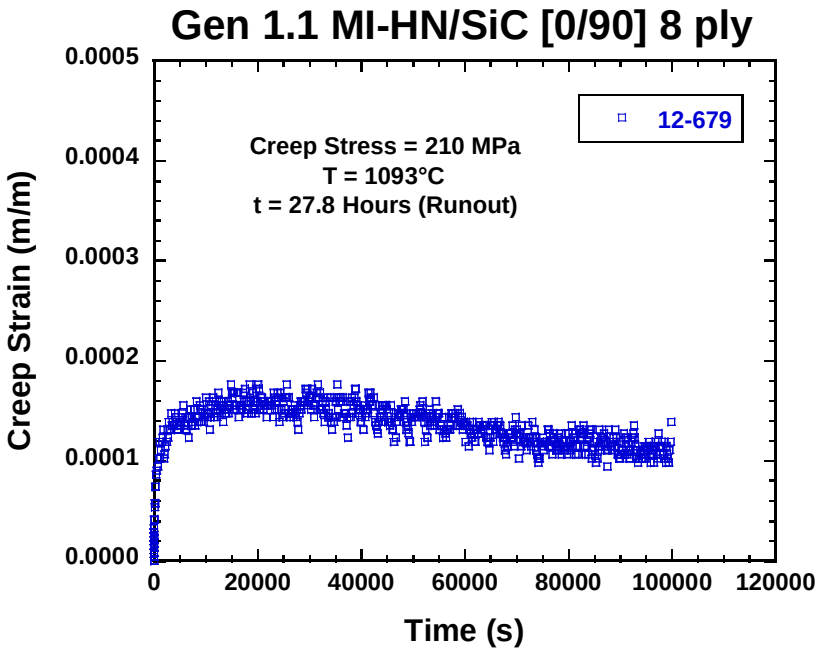

Figure 34. Creep strain versus time at 1093°C for a HiPerComp™ Gen 1.1 Hi-Nicalon/SiC (0/90)2s creep rupture run-out specimen

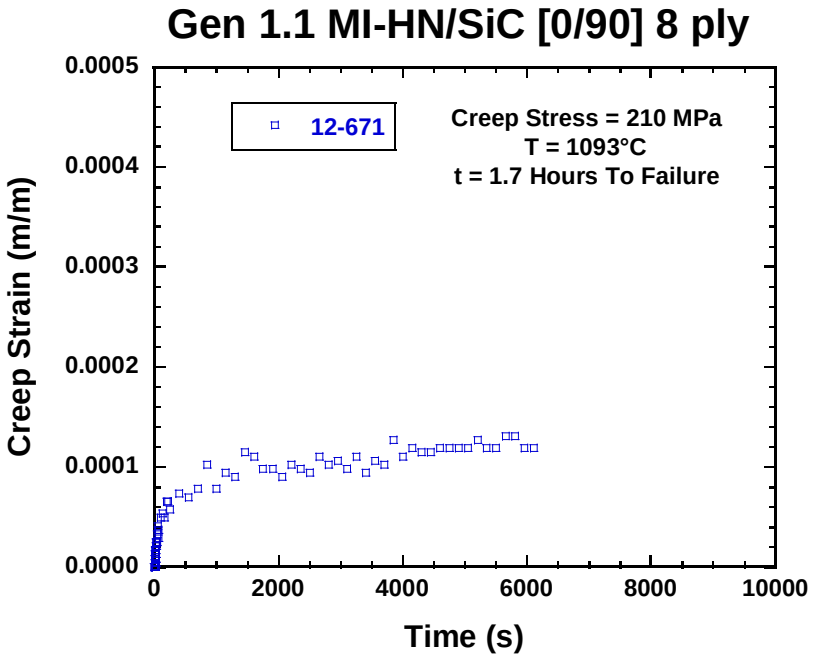

Figure 35. Creep strain versus time at 1093°C for the HiPerComp™ Gen 1.1 Hi-Nicalon/SiC (0/90)2s creep rupture specimen that failed

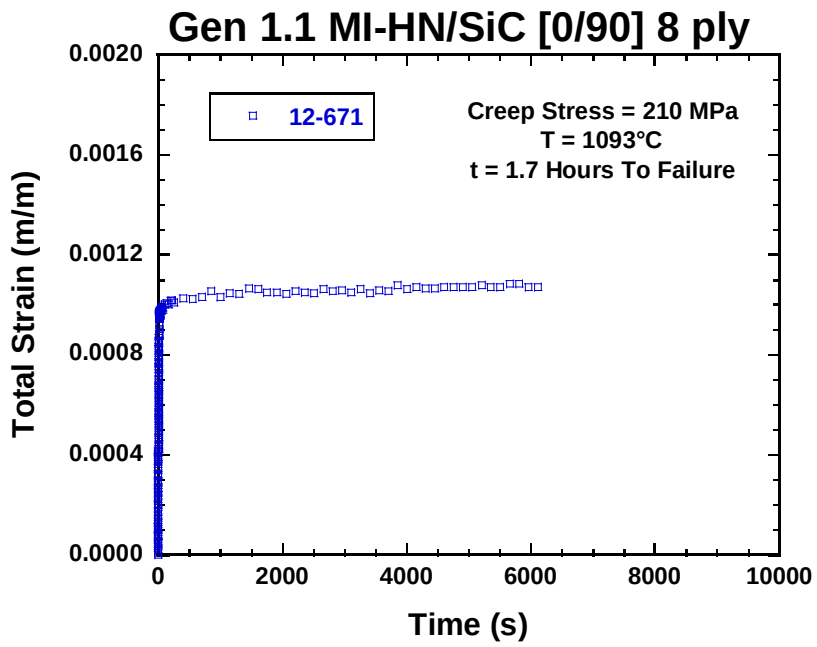

Figure 36. Total strain versus time at 1093°C for the HiPerComp™ Gen 1.1 Hi-Nicalon/SiC (0/90)2s creep rupture specimen that failed

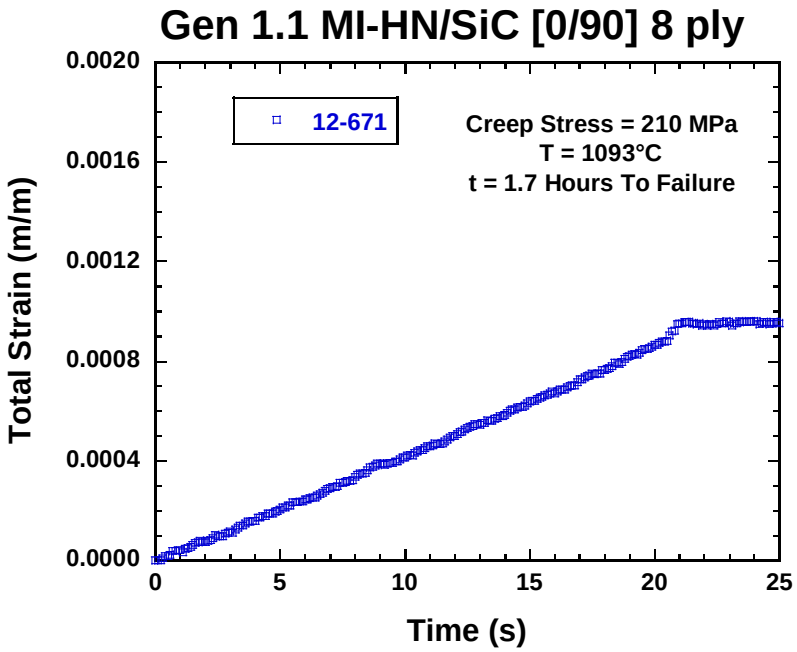

Figure 37. Expanded view of total strain versus time at 1093°C for the HiPerComp™ Gen 1.1 Hi-Nicalon/SiC (0/90)2s creep rupture specimen that failed

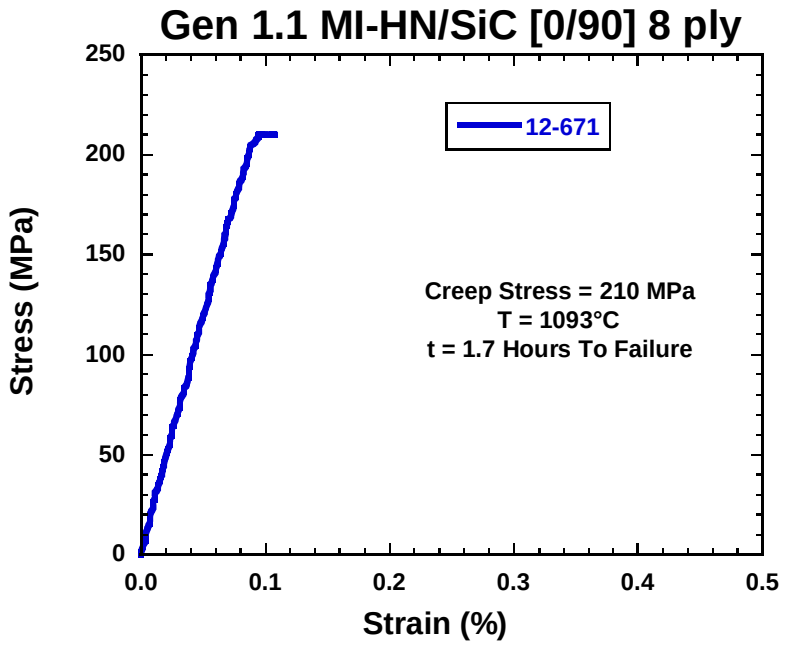

Figure 38. Plot of stress versus strain at 1093°C for the HiPerComp™ Gen 1.1 Hi-Nicalon/SiC (0/90)2s creep rupture specimen that failed

5.3. Durability Behavior

A table summarizing all of the durability test results is presented in Table 5. The table lists the test conditions and results, along with the measured tensile strength for those specimens that ran out (the column labeled RS). The results in Table 8 are presented in graphical form in Figure 39 as a plot of stress versus linear time to failure in seconds. From the plot, it is clear that the specimens fail either very early in life or reach run-out. The same data is presented in Figure 40 as a plot of stress versus log time in seconds. In observing the data in this figure it is very clear that failure time does not appear to be dependent on the type of test conducted. The only observation that can be made is that three of the 1000-second dwell fatigue specimens exhibited the three shortest lives. However, many more tests would need to be conducted to determine if there is a fatigue-creep interaction damage mechanism occurring.

The durability behavior demonstrated by the HiPerComp™ Gen 1.1 Hi-Nicalon/SiC material is very impressive. Most CMCs do not perform nearly as well at 1093°C and such high stress levels. Figure 41 shows unpublished fatigue test data (Zawada) at 1000°C for six different CMC systems. Three of the CMCs ran out at a stress level of only 50 MPa, while a fourth ran out at 100 MPa. The two oxide/oxide CMCs ran out at approximately 150 MPa. None of the six CMCs came close to running out at a stress of 200 MPa, even though the temperature was 1000°C, which is 100°C lower than the temperature at which the HiPerComp was tested. Figure 42 presents unpublished creep rupture data for the same CMCs but at 1100°C. As with the fatigue tests, none of these CMCs come close to matching the HiPerComp test data.

The durability data can also be presented as a bar chart, as shown in Figure 43. From these limited test data, it appears that a higher percentage of creep rupture specimens reached run-out.

This suggests the CMC may be ever-so-slightly more sensitive to cyclic loading compared to static loading. Again, much more work needs to be done to verify this observation.

The stress range over which the specimens failed or ran out was very small. Therefore, a plot of cross-sectional area versus time to failure was generated to determine if specimen measurement influenced the results. A specimen with a smaller cross-section would have had a lower applied load compared to a specimen with a larger cross-sectional area to achieve the same stress. If fiber volume fraction is the same, the specimen with the lower cross-sectional area should survive longer because the applied load is lower and hence the load on each fiber is lower. The results are shown in Figure 44. A quick look at the plot suggests there may be a trend in the data. The two specimens with largest cross-sectional areas had the shortest lives, while the two with smallest cross-sectional areas exhibited run-out at 100,000 seconds. However, specimens with a fairly large cross-sectional area also ran out, so no solid conclusions can be made between cross-sectional area and time to failure.

Table 5. Results from durability tests at 1093°C on HiPerComp™ Gen 1.1 Hi-Nicalon/SiC (0/90)2s

AFRL ID	GEA ID	Test Type	Test System	Test Date	Area (mm^2)	Stress (MPa)	Load (kN)	Time (hr)	Time (s)	Cycle Count	Failure Location Stress	RS (MPa)	Failure Locaiton (mm)
12-665	1852-02-003-3	Fatigue R=0.1, 1 Hz	SH12	4/22/2013	17.294	210	3.632	0.85	3,067	3,067	210.00	na	7
12-668	1852-02-004-1	Fatigue R=0.1, 1 Hz	SH12	5/30/2013	17.223	210	3.617	1.41	5,093	5,093	206.10	na	12
12-681	1852-02-004-9	Fatigue R=0.1, 1 Hz	SH12	4/24/2013	16.989	200	3.398	27.8	100,000	100,000	198.71	318.7	6
12-664	1852-02-003-2	Sustained Load	SH12	4/26/2013	17.317	210	3.637	27.8	100,000	na	204.99	305.7	15.5
12-669	1852-02-004-2	Sustained Load	SH12	5/28/2013	17.296	210	3.632	27.8	100,000	na	208.41	258.4	11
12-671	1852-02-003-9	Sustained Load	SH12	7/9/2013	17.34	210	3.641	1.7	6,112	na	208.03	na	1
12-679	1852-02-004-7	Sustained Load	SH12	7/11/2013	17.017	210	3.574	27.8	100,000	na	207.80	309.2	3
12-675	1852-02-004-3	Dwell Fatigue 10 sec hold	SH12	5/3/2013	17.32	210	3.637	5.04	18,152	1650	209.12	na	2.5
12-678	1852-02-004-6	Dwell Fatigue 10 sec hold	SH12	5/23/2013	17.137	210	3.599	27.8	100,000	9091	208.96	306	7
12-666	1852-02-003-4	Dwell Fatigue 100 sec hold	SH12	4/30/2013	17.244	210	3.621	9.2	33,027	327	209.11	na	6
12-667	1852-02-003-5	Dwell Fatigue 100 sec hold	SH12	5/21/2013	17.241	210	3.621	5.02	18,072	178	209.94	na	9.5
12-670	1852-02-003-8	Dwell Fatigue 1000 sec hold	SH12	5/7/2013	17.342	210	3.642	0.74	2,664	2	208.42	na	11
12-663	1852-02-003-1	Dwell Fatigue 1000 sec hold	SH12	5/7/2013	17.365	210	3.647	0.37	1,345	1	210.19	na	9.5
12-674	1852-02-004-2	Dwell Fatigue 1000 sec hold	SH12	6/2/2013	17.345	210	3.642	0.094	640	1	210.21	na	0
12-680	1852-02-004-8	Dwell Fatigue 1000 sec hold	SH12	7/3/2013	17.139	210	3.599	27.8	100,000	100	209.2	307.1	7.5

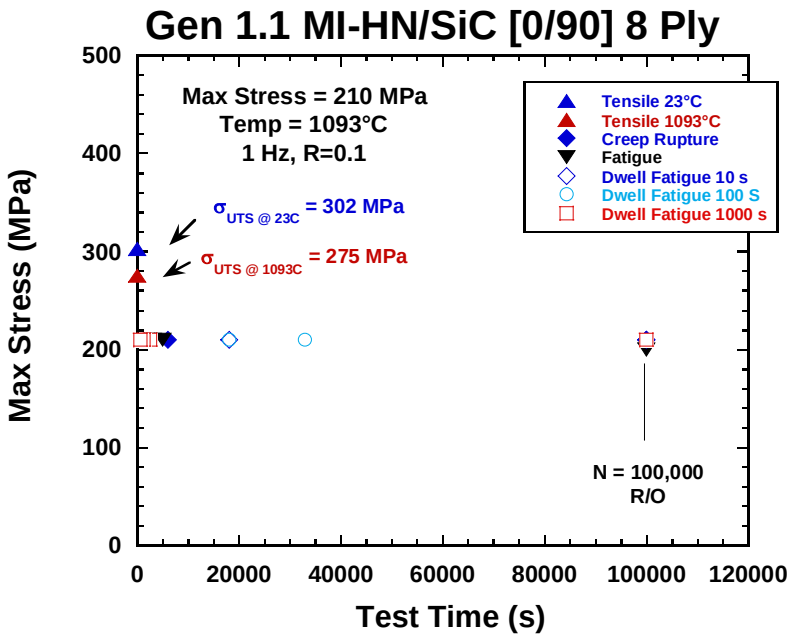

Figure 39. Maximum stress plotted against linear time to failure for HiPerComp™ Gen 1.1 Hi-Nicalon/SiC (0/90)2s

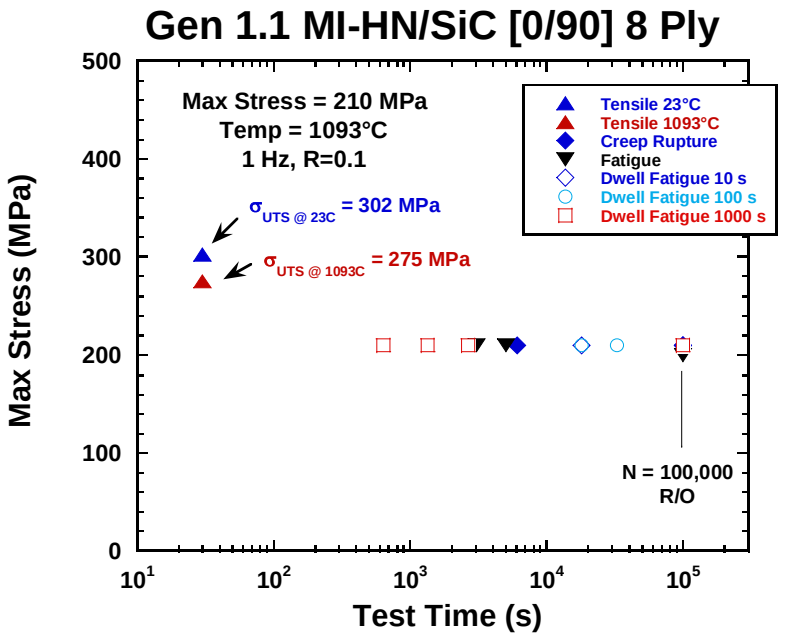

Figure 40. Maximum stress plotted against log time to failure in seconds for HiPerComp™ Gen 1.1 Hi-Nicalon/SiC (0/90)2s

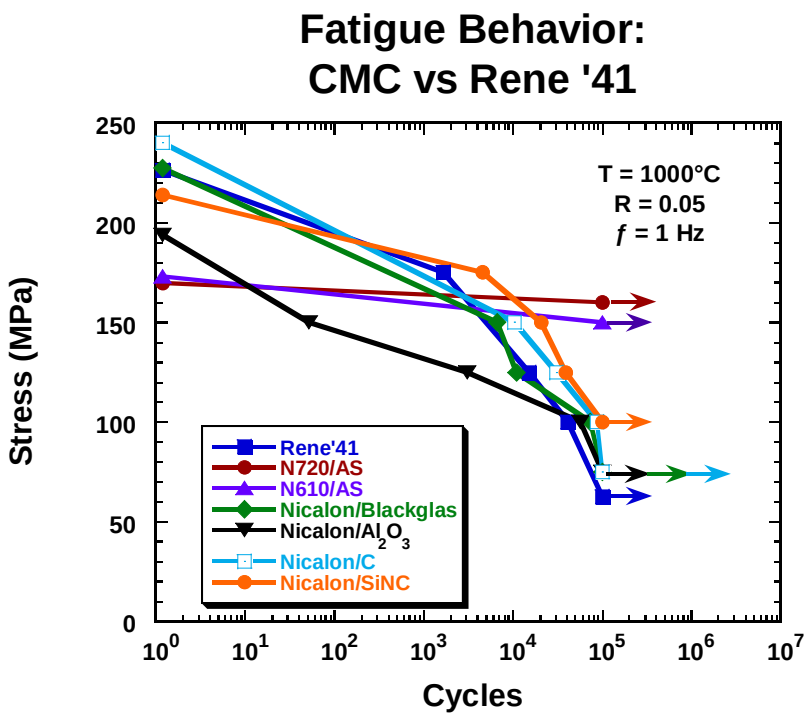

Figure 41. Stress versus cycles to failure for several CMCs fatigue tested at 1000°C

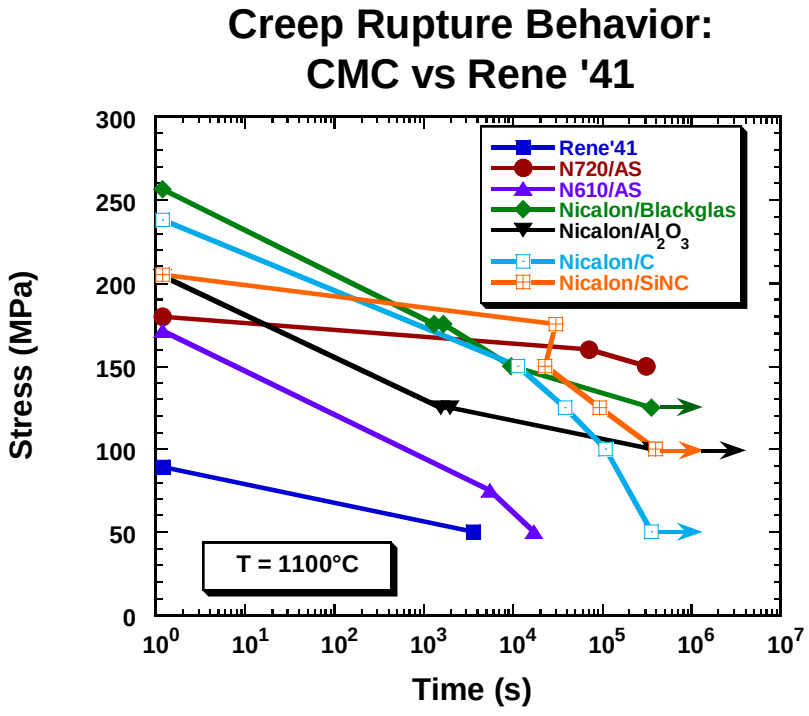

Figure 42. Stress versus time to failure for several CMCs creep tested at 1100°C

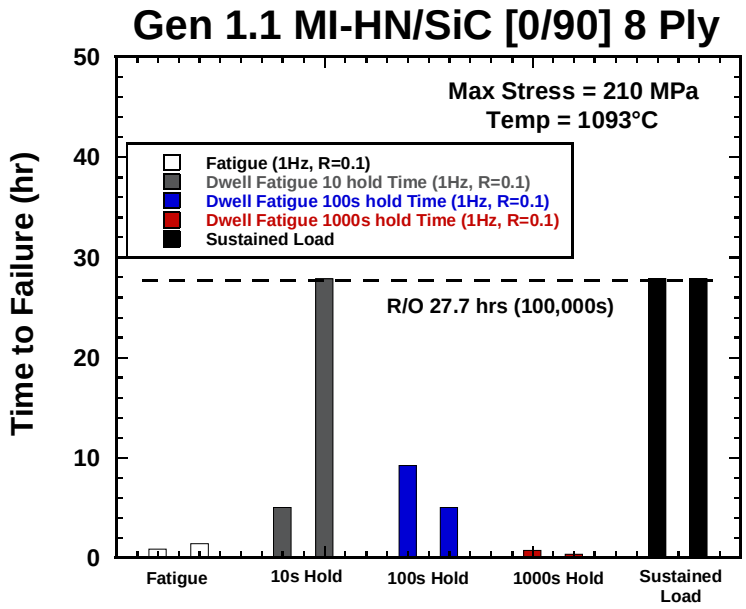

Figure 43. Bar chart of time to failure at 1093°C plotted against the test type/condition for HiPerComp™ Gen 1.1 Hi-Nicalon/SiC (0/90)2s

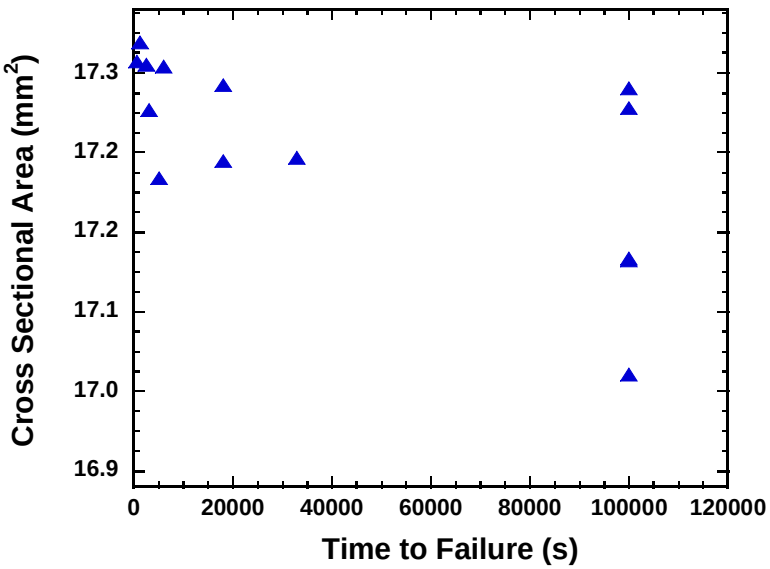

Figure 44. Plot of cross sectional area versus time to failure for all HiPerComp™ Gen 1.1 Hi-Nicalon/SiC durability specimens tested at 210 MPa and 1093°C

5.4 Residual Strength Tension Tests

The results of the tension tests conducted at room temperature on test specimens that had reached run-out are shown in Table 6. A very important finding is that all of these specimens had experienced 100,000 seconds at 1093°C, yet all exhibited residual tensile strength equal to or significantly higher than the room-temperature as-received strength value. The as-received strength was 268 MPa, while the specimens that ran out exhibited strength values that ranged from 258 MPa up to 319 MPa. This suggests that no damage occurred during any of the durability tests that ran out. In addition, the stress-versus-strain trace for 1000-second dwell is shown in Figure 45 along with the room-temperature as-received tensile stress-versus-strain trace. Thus, as long as the stress level is kept below the PL, this CMC does not experience any degradation in tensile strength upon subsequent loading.

None of the run-out specimens showed a reduction in modulus. The GE witness samples exhibited on average 270 GPa, and all of the run-out specimens exhibited similar values of stiffness. One surprising result was that the PL either remained constant or increased, in some cases by as much as 25 MPa. At this time, no explanation can be given. The strain to failure did decrease slightly for two specimens, and sharply for one of the creep rupture specimens (12-669). The as-received strain to failure was approximately 0.5%, and only one of the fatigue specimens exhibited more than 0.5% strain. So, the time at temperature under static loading appeared to decrease the strain to failure, while cyclic loading did not. However, much more testing needs to be done to confirm this effect.

Table 6. Room Temperature Residual Tensile Data for HiPerComp™ Gen 1.1 Hi-Nicalon/SiC Specimens That Had Reached Run-out During Durability Testing at 1093°C

Residual Strength: TTCP Gen1.1 MI-Hi-Nicalon/SiC							
Specimen ID	Test Type	Time (s)	Temp (C)	σ_{UTS} (MPa)	E* (GPa)	σ_{PL} (MPa)	ε_f (%)
12-681	Fatigue / 200 MPa / 1093°C	100,000	23	319	270	240	0.753
12-664	Creep / 210 MPa / 1093 °C	100,000	23	306	276	230	0.302
12-669	Creep / 210 MPa / 1093 °C	100,000	23	258	258	250	0.118
12-679	Creep / 210 MPa / 1093 °C	100,000	23	309	278	248	0.242
12-678	Dwell 10 s / 210 MPa / 1093°C	100,000	23	306	258	260	0.278
12-680	Dwell 1000 s / 210 MPa / 1093°C	100,000	23	307	271	250	0.313

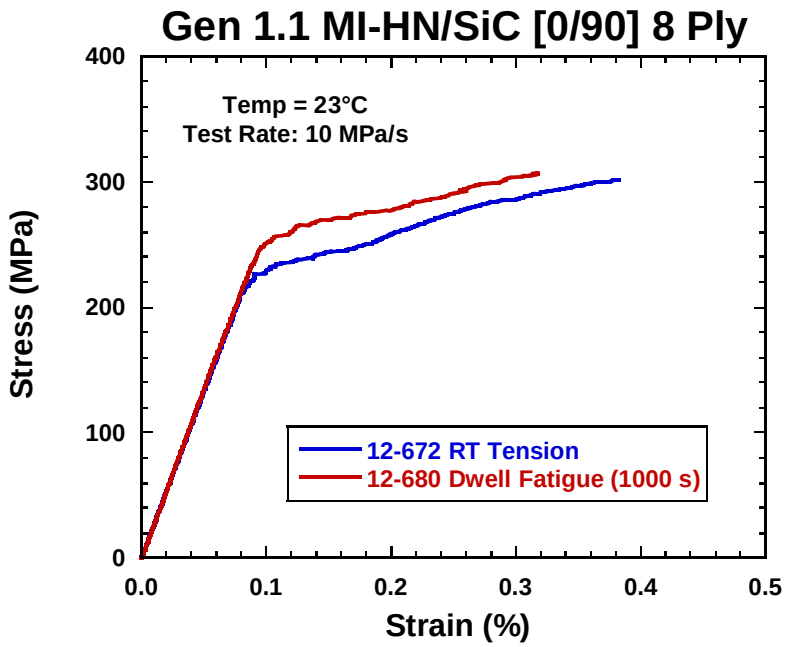

Figure 45. Room-temperature tension stress-versus-strain traces for HiPerComp™ Gen 1.1 Hi-Nicalon/SiC (0/90)2s comparing residual strength tensile behavior for a run-out 1000 second dwell fatigue specimen to the as-received tensile behavior

6.0 CONCLUSIONS

The test specimen design proved to work well for this CMC. All of the failures occurred in the machined gage section, with only one failing just at the start of the radius. None of the test specimens failed into the radius region. This is a very important finding and documents that, for these tests, there was no intermediate temperature embrittlement (ITE) occurring in this CMC. This is likely due to a very uniform and protective fiber coating and a very dense CMC matrix, thus mitigating easy oxygen ingress to the interior of the CMC. This is important, as this CMC had no exterior coating and the edges of the test bars were as-machined.

Tensile testing data at 23°C, 982°C, 1093°C, and 1204°C clearly showed that the HiPerComp^{TM} Gen 1.1 Hi-Nicalon/SiC (0/90)2s CMC should not be used above 1093°C. Tension tests conducted at 1204°C exhibited essentially no strain after reaching the PL, hence limited damage tolerance at this temperature.

Fatigue tests at 1093°C exhibited flat stress-versus-cycles-to-failure response. The specimen tested at 200 MPa ran out at 100,000 cycles at 200 MPa, and the two specimens tested at 210 MPa failed in a relatively short period of time. So, at this temperature, the fatigue limit was set at 205 MPa, which is below the identified PL of 225 MPa. This result indicates that there is some damage occurring below this PL. Significant work remains to identify the onset of matrix cracking in this CMC.

Creep testing at 1093°C and 210 MPa produced results similar to the fatigue testing. Three specimens ran out at 100,000 seconds, while one failed in only 6000 seconds indicating sensitivity to the PL. Therefore, the creep limit stress was approximately 205 MPa and is identical to the fatigue durability limit.

Dwell fatigue testing using hold times of 10 seconds, 100 seconds, and 1000 seconds at maximum load were conducted using a maximum stress level of 210 MPa. One 10-second hold specimen and one 1000-second hold specimen ran out while the remaining six test specimens all failed relatively early. Such a spread in test results indicates that there is no fatigue-creep interaction. It appears that the temperature is too low for this to occur. Hence the dwell fatigue durability limit was identified to be 205 MPa.

The window in stress level to either run-out or fail was found to be very small, about 5-10 MPa from the stress limit for all three types of testing.

The maximum stress limit to reach run-out was identified as 205 MPa for all three types of tests. This stress level is high compared to earlier generations of CMCs that have been fatigue tested at 1000°C. However, a stress level of 205 MPa is well below the identified PL of ~225 MPa (see Table 2).

All test specimens that ran out exhibited excellent retained tensile strength. This indicates that no significant damage occurred to the CMC during these 100,000-second tests at 1093°C. There were varying amounts of strain to failure, indicating some of the specimens were experiencing a slight degradation which did not alter ultimate strength, but did reduce strain to failure.

Specimens that ran out exhibited higher PL values compared to the as-received tensile properties. At this time, no explanation can be given.

The durability test results suggest that this CMC performed similarly in static loading and cyclic loading. Creep strain revealed that very little time-dependent deformation occurred. The results suggest that the main damage mechanism is crack initiation followed by crack growth.

7.0 RECOMMENDATIONS

The high temperature tensile behavior of this SiC/SiC CMC suggests that the maximum use temperature is 1093°C. Durability testing revealed a very sharp limit associated with the proportional limit of this CMC. Therefore, it is recommended that this CMC be used at stress levels below 205 MPa in order to avoid matrix cracking and subsequent failure during static or fatigue loading conditions.

8.0 REFERENCES

[1] GE Product Brochure #GEA-13712 (January 2004)

LIST OF SYMBOLS, ABBREVIATIONS, AND ACRONYMS

AFRL	Air Force Research Laboratory
ASTM	American Society for Testing and Materials
CMC	Ceramic Matrix Composite
DTIC	Defense Technical Information Center
GE	General Electric
ITE	Intermediate Temperature Embrittlement
HPT	High Pressure Turbine
E	Modulus
ε_f	Strain at Failure
IR	Infrared
MATE	Material Analysis And Testing
MI	Melt Infiltrated
MTS	Materials Test Systems
PL	Proportional Limit
RXCC	Composites Branch, Structural Materials Division of the Materials & Manufacturing Directorate
SiC	Silicon Carbide
UDRI	University of Dayton Research Institute
USAF	United States Air Force
UTS	Ultimate Tensile Strength